Performance Modeling, Design, and Analysis of Large Scale Terahertz Networks

Javad Sayehvand

A thesis submitted to the

Department of Electrical Engineering and Computer Science

in conformity with the requirements for

the degree of Master of Applied Science

YORK UNIVERSITY

TORONTO, ONTARIO

November 2020

Abstract

Multi-band and multi-tier heterogeneous networks have been considered as a key technology to meet the requirements of the future wireless networks; that is, 5G and beyond. In this dissertation, I studied heterogeneous cellular networks consisting of two tiers, where tier 1 is composed of small base stations (SBSs) operating on sub-6GHz spectrum, and tier 2 consists of dense deployment of Terahertz (THz) base stations (TBSs) with lower power transmission compared to the RF layer.

Using stochastic geometry (SG) tools, I modeled and analyzed the downlink performance of (i) THz-only network, and (ii) two-tier (co-existing) RF and THz network in terms of the downlink interference and coverage probability of a typical user. First, I characterized the exact LT of the aggregate interference and coverage probability of a user in a THz-only network. Then, for a coexisting RF/THz network, I derive the coverage probability of a typical user considering biased received signal power association (BRSP). In addition, asymptotic approximations are presented for scenarios where the intensity of THz BSs tends to infinity or molecular absorption coefficient in THz approaches to zero.

The proposed framework is generic to capture the performance of a typical user in various network configurations such as RF-only, THz-only, opportunistic RF/THz, and hybrid RF/THz. Finally, I extend the framework to incorporate the impact of

blockages and side lobe antenna gains. The derived theoretical results are validated through extensive Monte-Carlo simulations.

Acknowledgments

I would like to thank my advisor, Prof. Hina Tabassum, for her continuous support and encouragement. Thank you Dr. Hina, for giving me the opportunity to be a part of your team. You supported me greatly and were always willing to help me not only during the course of my graduate research but also in many life's difficult moments over the past two years. My sincere gratitude to my supervisory committee members Prof. Ping Wang and Prof. Rashid Bashir for their time, constructive comments, and feedback that helped me improve my dissertation.

I am also grateful to have my parents for their never ending love, kindness and support. There are not enough words to describe how thankful I am to have both of you. Thank you for always being there for me. I would also like to thank my siblings whose voices over the phone make me forget everything and just smile. I am immensely thankful to have Maryam, my love and my life partner by my side. You are the most amazing person in my life. Thank you for taking care of me beyond my dreams and expectations. Thank you for always being there for me through thick and thin.

Contents

List of Figures

Chapter 1

Introduction

1.1 Evolution of Wireless Networks (1G-5G)

Telecommunication and networking, i.e., the wireless transmission of the data had a significant role in the advancement of people's life-style. During the past decades, this technology itself has been subjected to evolutionary changes from the first generation (1G) – the earliest form of voice-only network – to the current fifth-generation (5G) Fig. 1.1. Incentives such as high data-rate, low latency, higher energy-efficiency, improvement in the quality of service, and network compatibility have always been the main reasons of the evolving wireless networks towards the next generations.

For instance, 1G networks provide voice-only connections. The second-generation (2G), lasting from 1980s to 2003, includes networks such as Global System for mobiles (GSM), General Packet Radio Service (GPRS), and Enhanced Data rates for GSM Evolution (EDGE). GSM provides data transmission as a speed in the range of 30-35 kbps, GPRS with some refinements provides a data rate at the order of 110 kbps. EDGE that can be also be known as 2.9G or 3G results in significant improvements in the data rate over GSM and GPRS. This network is even being used on many

mobile networks, as it meets the basic requirements of both users and carriers. The significant revolution in wireless networks happened when technologies such as Code-division multiple access (CDMA) has been introduced. Third generation (3G), being based on CDMA2000 and EDGE, has speed capabilities of up to 2 Mbps. Thus, applications such as sending/receiving large emails and texts, fast web browsing, and video streaming that once were hindered became a reality.

Afterwards, fourth-generation (4G) with requirements such as integrating Internet Protocol (IP) for data traffic and minimum data rates of 100 Mbps enabled a significant transition from 3G. 4G is always being referred to as MAGIC, meaning that 4G provides several features such as mobile multimedia with high data rates, global mobility support, integrated wireless solution, customized personal service, etc. Soon after, Long Term Evolution (LTE), which is a complete redesign and simplification of 3G network architecture, was introduced. In this network, latency is decreased significantly, and subsequently, spectral efficiency and communication speed increased.

Yet, there are several emerging wireless applications such as virtual reality, online gaming, vehicular/aerial/underground communications, tactile communications that require a higher data rate and lower latency to be enabled. What is more, in the current and the future world, the number of sensors required for gathering data from any kind of sources is skyrocketing. The connection of such devices to an operational center or with each other has resulted in the introduction of The Internet of things (IoT). Besides, traditional communication channels such as Zigbee and LoRA in IoT networks may not handle high data rate and latency-sensitive applications. Therefore, IoT networks can leverage on the wireless cellular networks for resource intensive and latency-sensitive applications.

Table 1.1: Major requirements of the 5G networks [6]

Type	Data Rate	Latency		Reliability	Connectivity
		E2E	Radio-only		
4G	$\sim$ 1 Gbps (SE: bps/Hz/m^2)	$\sim$50 msec	$\sim$ 5 msec	four-nines	2000 connected devices per .38 square miles
5G	$\sim$ 10-20 Gbps (SE: bps/Hz/m^2)	$\sim$ 5 msec	$\sim$ 100 nsec	five-nines	1 million connected devices per .38 square miles
B5G/6G	$\sim$ 1 Tbps (SE: bps/Hz/m^3)	¡1 msec	$\sim$ 10 nsec	seven-nines	1 trillion connected devices per .38 square miles

Among all the above requirements, the increase in the data rate and reduction in transmission latency is the most crucial key performance indicators (KPIs) in wireless mobile networks. Technologies such as ultra-densification, millimeter Wave (mmWave), and massive multiple-input multiple-output (M-MIMO) - " big three"- has been suggested as solutions to this problem [3,4]. In ultra-densification solutions, more radio base stations are deployed in an area to increase the number of users that can be served. In the M-MIMO solution, each base station is equipped with a large number of antennas more than what is practiced in the LTE now. Moreover, given that the sub-6GHz frequency is congested and limited, and there is a big crunch of unlicensed spectrum available in high frequencies, migration to the higher frequencies such as mmWave can provide much higher data rates. The mm-wave band has already been investigated in various research works, and it is being used in 5G network prototype worldwide and some companies have produced 5G smart-phones such as Samsung Galaxy S10 [5].

I summarize the KPIs of 4G, 5G, and 6G networks in Table 1.1.

1.2 Introduction to 6G

Despite the aforementioned advancements, the global mobile traffic volume is expected to grow from 7.462 exabyte per month (EB/month) in 2010 to 5016 EB/month

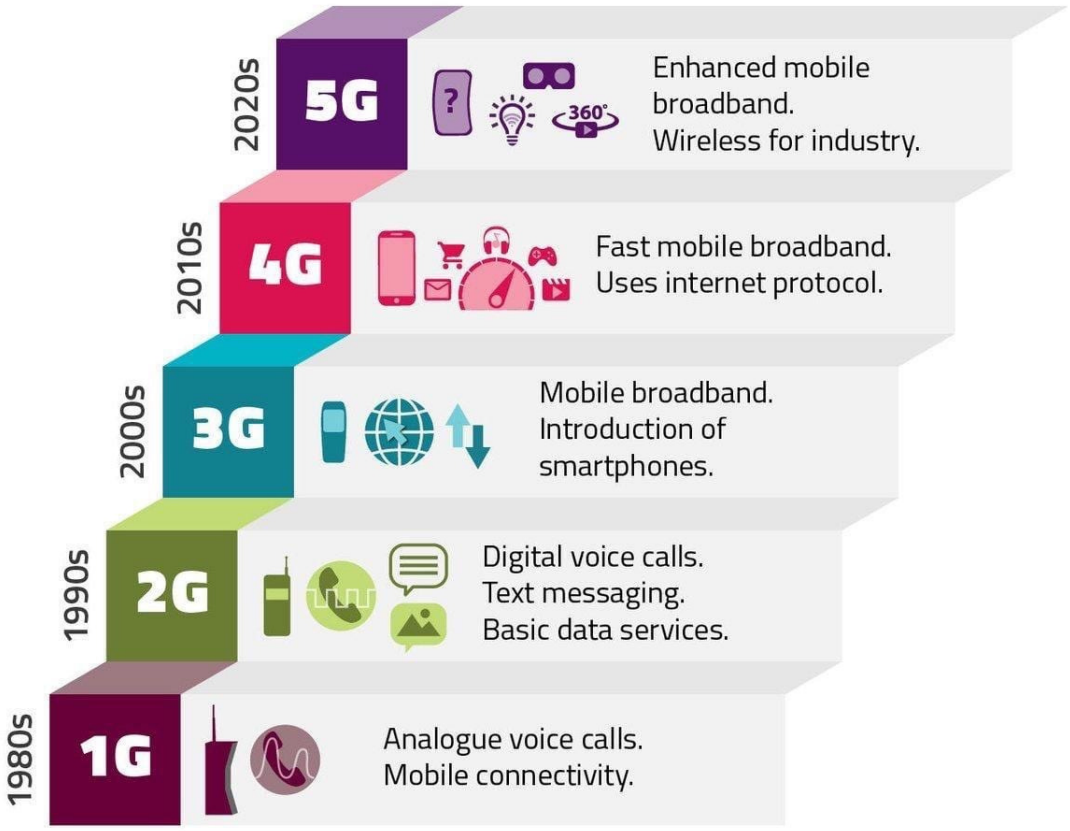

Figure 1.1: Evolution of wireless networks from both research and commercialization perspective [1]

in 2030 [7]. Yet, it is difficult for the millimeter wave (mmWave) transmissions to achieve data rates in the order of Tbps, impeded by the total consecutive available bandwidth of less than 10 GHz in the mmWave systems. Thus, the launch of sixth-generation (6G) wireless networks is inevitable. 6G networks will observe coexisting RF and mm-wave deployments [8] and coexisting RF and visible light communication (VLC) [9, 10] deployments. In addition, higher frequencies in the THz band [0.1-10 THz] will be central to ubiquitous wireless communications in 6G. Other key highlights of 6G will be cell-free network architectures, holographic/ultra-massive MIMO,

three dimensional (3D) connectivity enabled with unmanned aerial vehicles (UAVs), virtual network slicing, large intelligent surfaces (LIS), and machine learning enabled resource allocation.

Higher frequencies (such as millimeter waves in 5G and THz in 6G) will offer ample spectrum, multi Gigabit-per-second (Gbps) data rates, and highly secure transmissions. Fortunately, recent advancements in the electronic and photonic technologies, which are based on up-conversion of microwave and mm-wave signals or down-conversion of optical signals, have brought the hope to produce transceivers that can support THz (0.1-10 THz) communication. Added to this, the recent usage of nano-material such as graphene, has opened a new door to develop THz equipment that can support THz wireless communication. Thus, THz communication which was once impeded due to lack of proper devices is open for more explorations.

1.3 Significance of THz Spectrum in 6G

THz frequencies are identified by the US Defense Advanced Research Projects Agency (DARPA) as "*one of the four major research areas that could eventually have an impact on our society larger than that of the Internet itself*". Beyond traditional applications of wireless networks, THz can support systems with "billions of connected nanosystems" and has been identified as *"one of the four essential components of the next IT revolution*" by the Semiconductor Research Consortium (SRC) and the US National Science Foundation. THz systems are expected to be beneficial not only for traditional macroscale wireless networks but also for emerging paradigms such as wireless intra- and inter-chip communications, nano-communications, and the Internet of

Bio-Nano Things. SRC sponsored research on the convergence of THz communications and sensing technologies for future cellular infrastructure. The U.S. Federal Communications Commission (FCC) already opened the THz band for research purposes in 2019. The International Telecommunication Union (ITU) Telecommunication Standardization Sector (ITU-T) Study Group 13 established the ITU-T Focus Group Technologies for Network 2030. The potential of using THz in the 6G wireless networks is evident [11]. In this context, multiple leading 6G initiatives probe THz communications, including the "6Genesis Flagship Program (6GFP)", the European Commission's H2020 ICT-09 THz Project Cluster, and the "Broadband Communications and New Networks" in China.

1.4 Benefits and Challenges of THz Transmissions

THz has four features of paramount importance, making it one of the key technologies towards the Tbps communication networks. These features include: (i) ample spectrum resources up to hundred of GHz; (ii) the wavelength of this frequency is small enough to implement miniaturized antennas, bringing about the integration of thousands of THz antennas; (iii) the symbol-level-duration is about pico-second, resulting in distortion resistant communication; and (iv) enhanced security due to limited transmission range [12]. THz frequencies (0.1-10 THz) can potentially enable sophisticated applications (e.g., virtual reality and augmented reality, vehicular networks, industry 4.0, etc.) that require agile, reliable, and almost zero latency transmissions. Moreover, THz enables nano-system applications such as network-on-chip communications (WiNoC) and the Internet of Nano-Thing (IoNT).

Despite the promising opportunities THz provide for the future wireless communication, there are some challenges that can impede the performance of THz communications. The main challenges include higher channel propagation losses resulting from a variety of impediments including molecular absorption. Moreover, THz transmissions will be highly directional, thereby making it susceptible to the line-of-sight (LOS) blockages constraining the communication range. Thus, the coverage zones are limited compared to RF (sub-6GHz), and THz spectrum can be considered as a complementary spectrum to the conventional RF spectrum.

1.4.1 Transceiver Implementation

THz sensing has been considerably studied back to the 1990s, but due to less compact high-power transmitter and high-sensitive detector, which are proper for operating at room temperature, application of THz in wireless communications has been handicapped for a long time. Fortunately, many recent advancements in electronic and photonic technologies as well as the knowledge of nanomaterial have paved the way to fill the so-called *THz gap*. In the following, I discussed them separately:

- From the electronic perspective, the significant advancements in the technologies of standard silicon CMOS , silicon-germanium BiCMOS, and III-V semiconductor-based High Electron Mobility Transistor (HEMT), metamorphic HEMT, Heterojunction Biopolar Transistor (HBT) and Schottky diode have made them suitable enough to produce sources, amplifiers and mixers, which can operate at frequencies close to 1 THz. Thus, using the up-conversion technique, THz signals can be generated from lower frequencies by means of frequency multiplier chains. The generated signals can achieve a power of the order of hundreds

of milliWatts (mWs) at 240 GHz to a few mWs at 1 THz.

- From the photonic aspect, technologies such as optical down-conversion systems based on photomixers or photoconductive antennas, uni-traveling carrier photodiodes (UTC) and quantum cascade lasers (QCLs) have witnessed unparalleled progress, making these technologies a potential enabler for the THz implementation. The lower power of the optical system is a disadvantage compared to the electronic systems. However, signal processing in photonic devices can be done more faster than electronic technologies, which is advantageous compared to electronic systems. Thus, the best solution might be the integration of photonic and electronic systems for the receiver and transmitter parts, respectively.

- On top of all aforementioned advancements, nanomaterials such as graphene can be used for THz communication systems. The small size of these devices enables them to operate efficiently at THz frequencies and support very large communication bandwidths. Moreover, the direct generation of THz signal is feasible using the graphene/III-V semiconductor device, which is different from photonic and electronic technologies, based on the up-conversion of microwave and mm-wave signals or the down-conversion of optical signals. Finally, the lack of energy loss through harmonics enhances the efficiency of THz communication systems.

1.4.2 Channel Propagation Losses in THz

Understanding the propagation features of any transmission medium is the fundamental step towards designing efficient channel coding schemes, modulation/demodulation

Table 1.2: Key Channel Impairments in THz Communications

Parameter	**Dependence on frequency**	**Impact on 6G THz systems**	**THz vs. Microwave and FSO**
Spreading Loss	Quadratic increase with decreasing area and constant gains; Quadratic decrease with constant area and frequency-dependent gains	Distance limitation	Higher than microwave, lower than FSO
Atmospheric Loss	Frequency-dependent path loss peaks appear	Frequency-dependent spectral windows with varying bandwidth	No clear effect at microwave frequencies, oxygen molecules at millimeter wave, water and oxygen molecules at THz, water and carbon dioxide molecules at FSO
Diffuse Scattering and Specular Reflection	Diffuse scattering increases with frequency. Specular reflection loss is frequency-dependent	Limited multi-path and high sparsity	Stronger than microwave, weaker than FSO
Diffraction, Shadowing and LoS Probability	Negligible diffraction. Shadowing and penetration losses increase with frequency. Frequency-independent LoS probability	Limited multi-path, high sparsity and dense spatial reuse	Stronger than microwave, weaker than FSO
Weather Influences	Frequency-dependent airborne particulates scattering	Potential constraint in THz outdoor communications with heavy rain attenuation	Stronger than microwave, weaker than FSO
Scintillation Effects	Increase with frequency	Constraint in THz space communications	No clear effects at microwave, THz is less susceptible than FSO

schemes, resource management schemes, user assignment schemes, to name but a few. To this end, the THz channel propagation has been widely studied and there is comprehensive channel modeling for THz band in [13]. The THz channel propagation is susceptible to free-space path losses (which is composed of spreading loss and molecular absorption), blockages of different types (e.g., wall blockers, dynamic human blockers, self-blockage), diffraction and scattering, weather influences, scintillation, etc. In the following, I briefly describe the main impediments of THz propagation. A summary is provided in **Table 1.2**.

1.4.2.1 Free-Space Propagation

Free space path loss is made up of spreading loss as well as atmospheric loss, that is, molecular absorption loss.

- *Spreading loss:* There are two models for spreading loss. When the antenna gains are frequency-independent and the antenna aperture at the transmitter and receiver reduces with the increasing frequency, the spreading loss decreases quadratically with frequency, the same as Friis' law. However, when the antenna aperture at the transmitter and receiver are constant, and gains are frequency-dependent, the spreading loss shrinks with the square of frequency. In general, the former model is considered for the analysis in THz Band, and [14] reported that in the distance of 10 meters, the spreading loss is about 100 dB, resulting in a tough long-range communication in this band.

- *Atmospheric Loss or Molecular Absorption Loss:* As the frequency of electromagnetic waves increases, the probability with which the particle of these waves collides with the gas molecules in the propagation medium increases. This kind

of loss does not have any effect at microwave frequencies. However, it is observed at mmWave due to oxygen molecules, at free-space optic (FSO) band due to water vapor and carbon dioxide, and in THz band, due to both the water vapor and oxygen molecules. This phenomenon is known as molecular absorption loss.

1.4.2.2 Diffraction, Scattering, Shadowing, and Line-of-Sight

As the frequency increases the signal absorption will increase, resulting in a reduction in the diffraction signal. Thus, the effect of diffraction path can be neglected in high frequencies, and especially THz. As to the shadowing, this effect will be noticeable, since when a THz is blocked its energy will be absorbed totally. Finally, the LoS link only follows Friis' law.

1.4.2.3 Blockages

The blockage between a user and its associated base station in wireless communication systems is caused due to three main reasons: the blockage due to the user itself, also known as self-blockage, the blockage due to other human movements, and other static blockages including trees, indoor constructions such as walls, objects, etc. In the following, I will briefly describe the aforementioned blockages.

- *Self-Blockage:* self-blockage can have a significant effect on the performance of THz communication systems. In this kind of blockage, signals from the surrounding base stations even if they are within the close proximity of a user may be blocked by the user itself. The area in which signals from users are blocked by themselves is defined as "self-blockage zone" [15] and [16].

- *Dynamic Human Blockers:* In any wireless communication system, and especially in higher frequency bands such as mmWave and THz, moving humans act as blockers. They not only can block the link between a user and its associated base station, but also they block the signals from interfering base stations. Normally, these blockers are considered as moving cylinders, their locations follow a Poisson Point Process (PPP) in which the mobility of the blockers follows the random directional model (RDM) with constant moving speed [17–19]. Confirming with the RDM model, the probability density function of (PDF) human moving blocker is uniform over time [20]. Thus, the location of human blockers can be modeled as PPP.

- *Wall Blockers:* Walls are significant blockers in THz indoor transmissions and are normally modeled as a Boolean rectangles. The rectangles can be generated using Boolean scheme of straight lines [21, 22]. The length of walls can be assumed to follow an arbitrary PDF, and the center of them follows a PPP. Due to the fact that the widths of walls are much smaller in comparison to the length of the walls, the width are ignored normally. The orientation of walls is assumed to be a binary choice of either 0 or $\pi/2$ with binomial PDF.

.

1.4.3 Molecular Noise

The molecular absorption will cause the internal vibration of molecules and this vibration will radiate an additional signal in the same frequency. This additional signal is known as molecular absorption noise [23].

1.4.4 Interference Modeling in Large-Scale THz Network

As mentioned above, the THz band possesses challenging channel propagation characteristics (e.g., molecular absorption) that makes it different from well-studied bands such as RF and mmWave. Mathematically speaking, the received signal power is a function of the free-space path-loss as well as spreading loss which is modeled as the exponential function of the distance between transmitter and receiver. Therefore, when it comes to the performance analysis of a randomly located user in THz wireless networks, it is challenging. Moreover, since THz networks are intrinsically short-range, they will be deployed on large-scale (e.g., ultra-dense networks). Therefore, interference modeling becomes even more challenging than the traditional networks, since interference analysis should take into account a large number of sources of interferers due to high density, and analyzing the statistics of such a random variable becomes challenging than ever before.

1.4.5 Multi-band (or Coexisting) RF and THz Network

The conventional RF spectrum is characterized by strong transmission powers and wider coverage; however, the spectrum is limited and extremely congested. Channel propagation at higher frequency bands (e.g., THz and mmWave) is susceptible to shorter transmission distances, absorption, blockages, atmospheric gaseous losses due to oxygen molecule and water vapor absorption, rain losses, and penetration issues [24–26]. That is, THz and mmWave networks have reduced coverage range but plenty of spectrum, so there exists a trade-off based on users' requirements, users' density, and available spectrum. Compared to conventional radio frequency (RF),

THz transmissions incur high propagation loss thus significantly limiting the communication distance.

Thus higher frequencies are complementary to the conventional RF spectrum and the need of analyzing multi-band or coexisting networks is evident. Subsequently, the scope of this thesis is limited to analyzing the performance of users in coexisting RF and THz 6G networks. To date, a handful of research works have considered analyzing multi-band networks [9].

1.5 Motivation and Contribution

To my best knowledge, none of the existing research works presented a comprehensive analytic framework to characterize the exact interference statistics and coverage probability of users in a THz-only network or a coexisting two-tier RF and dense THz network (i.e., where the intensity of THz TBSs can be significantly high compared to the conventional RF SBSs. Thus, my contribution to this end is summarized as follows:

- *LT of the aggregate interference:* Deriving the LT of interference is a crucial step in analyzing the network's performance. Due to the propagation features of lower frequency bands, extracting LT of interference in these bands is pretty straight-forward. Yet, the extraction of LT in THz networks is challenging, and some research works have mentioned that it is impossible and adhered to numerical tools for calculation of mean interference [27]. Yet, I have come up with a novel, exact and closed-form expression to characterize the LT of the interference in THz band.

- *THz-only coverage probability:* As a performance metric, coverage probability

always has been of interest in wireless mobile networks. Yet, previous studies as to the coverage probability of THz mentioned that extracting a closed-form and exact formula for coverage probability is hampering. Yet, I have proposed an exact and closed form expression to evaluate the coverage probability in THz-only networks.

- *Association probability:* In the current thesis, I have assumed a two-tier network, including RF and THz tiers. In such networks, it is important to know the probability with which a user can associate to a tier. Thus, I have extracted an exact and closed formula for association probability to each layer.

- *Association probability:* Further, I have considered two asymptotic cases for the density of base stations in THz band, proposed more simple formulas for the asymptotic cases.

- *Distance distribution:* In traditional heterogeneous networks, the distribution of user's distance from a specific tier is derived considering RF-only transmissions at both tiers. Nonetheless, due to the distinguishing characteristics of THz, the distance distributions in heterogeneous networks are not applicable here. Thus, a new formula should be extracted for the distribution of users to its tagged BSs in the THz/RF setup. To this end, I have derived an exact formula for distance distribution in coexisting THz/RF setup.

- *Coverage probability for coexisting RF/THz setup:* Finally, by considering the previous analysis such as association probability, distance distribution, with the help of Gil-Pelaez inversion theorem an exact formula for the coverage probability in a two-tier network, consisting of one RF and one THz layer, is extracted.

Chapter 2

Background and Literature Review

In this chapter, an overview of stochastic geometry, point processes, and general concepts that are commonly used to characterize the performance of wireless mobile networks are provided. These mathematical preliminaries are provided so that one has enough knowledge to follow the discussions and calculations in the following chapter. Thus, if the reader is familiar with the stochastic geometry tools, the reader can move to the literature review section of this chapter.

2.1 Evolution of Heterogeneous Networks

Almost a decade ago, hexagonal grid was the main approach used to model wireless mobile networks. In this setup, mobile users are distributed in a deterministic manner or according to Poisson point processes (PPPs) [28–31]. Although these approaches were widely used to analyze the traditional homogeneous wireless networks including, 1G, 2G, and 3G, the approach is oversimplified and was intractable as well. For example, to calculate specific key network performance indicators such as coverage probability or reliability for a target rate or average data rate heavy computations and simulations are needed to be executed.

The fourth generation of wireless mobile networks was supposed to support a huge amount of data traffic generated by humans. However, the 4G network encountered the problem of spectrum scarcity both in the available licensed and unlicensed radio spectrum. Towards this end, heterogeneous networks with the random deployment of lower power BSs with lower coverage zones such as micro BSs, pico BSs, femto BSs, aggregators, phantom BSs, and relays are considered as the solution to enhance spectral reuse. Nevertheless, the performance modeling and analysis of heterogeneous networks became analytically cumbersome due to the heterogeneity of BSs and irregular coverage zones. Thus, the performance cannot be analyzed using traditional mathematical modeling tools in a straight-forward manner.

Subsequently, the need for a tractable mathematical tool for modeling, designing, and analyzing heterogeneous networks became more evident. Further to the 4G network, 5G and beyond networks are also identified by the randomness and heterogeneity due to the deployment of ultra-dense base stations. In this context, stochastic geometry has emerged as a powerful tool to capture the irregularity and heterogeneity in the deployment of cellular networks. Stochastic geometry allows the locations of the base stations and mobile users to be modeled using point processes, thereby enable efficient modeling, design, and analysis of the wireless networks.

2.2 Key Performance Indicators

The primary performance metrics that are being used to analyze the performance of wireless mobile networks are defined as follows:

- *Coverage probability:* is defined as the probability that the received SINR at a specific user is larger than a predetermined threshold. Thus, the coverage

probability $\mathbb{P}_C$ can be defined as $\mathbb{P}_C = \mathbb{P}\,(\text{SINR} > \text{threshold})$, and consequently outage probability can be given as $\mathbb{P}_{\text{out}} = 1 - \mathbb{P}_C$.

- *Spectral efficiency:* is defined as the average data rate at which data can be transmitted over a given bandwidth. The spectral efficiency is a function of SINR and is defined as $R = \log_2(1 + \text{SINR})$.

- *Mean local delay:* is defined as the average amount of time that is required for the successful transmission of a packet from a transmitter to its associated receiver over a communication channel. The delay is related to coverage probability and is defined as $\frac{1}{\mathbb{P}_C}$.

- *Spectral frequency reuse efficiency:* defines how many times a frequency band has been used over the spatial domain of the entire network.

- *Energy efficiency:* is defined by the amount of data, that is, the data rate at which data can be transmitted from a transmitter to its associated receiver per unit power consumption.

- *Link reliability:* is defined by the fraction of users that can achieve $x\%$ probability for successful transmission. Thus, link reliability will be defined with a conditional probability density function for the probability of successful transmission at a specific link.

As we can see in the above metrics, SINR plays a vital role in the definition of all KPIs. Thus, in the following, a brief definition of SINR is presented.

2.2.1 Signal to Interference Plus Noise Ratio (SINR)

In the wireless mobile networks, the transmit signal will be modulated and coded before sending over the channel. The received signal will experience both large-scale and small-scale fading. Consequently, the received signal can be given as follows:

$$\mathrm{y}_r = x_t \gamma h + n_0, \tag{2.1}$$

where x_t is the transmitted signal, h is the small-scale fading between a user and its tagged BS, and finally, γ is the large scale fading, which is dependent on the operating frequency, and its distance to the serving BS.

When a set of transmitters are transmitting over a channel, the received signal at the desired receiver will become:

$$\mathrm{y}_r = x_{t,0} \gamma_0 h_0 + \sum_{i \in \mathcal{I}} x_{t,i} \gamma_i h_i + n_0, \tag{2.2}$$

Finally, the received SINR expression is given as follows:

$$SINR = \frac{P_t\left(x_0\right) H_0 \gamma_0}{N_0 + \sum_{i \in \mathcal{I} \backslash 0} x_{t,i} \gamma_i H_i}, \tag{2.3}$$

where $\mathcal{I} = \{x_0, x_1, x_2, \cdots\}$ includes all users in the network, and H_i, $i =\in \{0, 1, 2, \cdot\cdot\cdot\}$ denotes the channel power.

2.2.2 Shannon Limit

Data rate is another important metric that can be used to measure the performance of the wireless networks. According to the Shannon limit, the data rate of the wireless

mobile networks is bounded by the capacity of the network, that is:

$$R < C, \tag{2.4}$$

where C is the capacity of network and it is defined as:

$$C = M\left(\frac{W}{N}\right)\log_2(1+SINR) \quad \frac{bits}{sec}, \tag{2.5}$$

where W is the available spectrum bandwidth at the BS, N is the number of mobile users that are connected to the BS, and M is the number of spatial data streams (i.e., spatial multiplexing) between the base station and its tagged users. According to **Equation 2.5**, in order to increase the capacity of mobile networks, three factors are crucial, including the number of BSs, channel bandwidth, and spatial multiplexing gain.

2.3 Stochastic geometry

Stochastic geometry is a strong mathematical tool to study large-scale network performance and interference analysis. Referring to 2.3, SINR crucially depends on the distance between a user and its serving base station. In addition, user mobility and unplanned radio access points (RAPs) installation brings about randomness and uncertainty in wireless mobile networks. Moreover, the geometry of the location of the transmitter and receiver plays a significant role in the performance analysis of the wireless mobile networks. Thus, in order to capture the properties of wireless networks and analyze the performance of them, I resort to SG, a strong mathematical tool to model the spatial location of points. Since, I have used SG substantially

through the thesis, the basics concept of SG are explained in the following of this chapter. The fundamental concepts provided here are enough for the readers to understand the flow of my analysis in the thesis, but for more information as to SG, any avid reader can refer to [32–34].

- *Point process:* A deterministic sequence of points can be expressed as $\kappa = (x_k)_{k\in\mathbb{N}}$, where $\mathcal{N}$ is the space of sequences. In addition, if $\mathcal{N}$ is the output of a random process, the space of the sequences will be a *point process*. A more formal definition of a point process is provided in [33], and as stated in [34], "a point process is a random collection of points that resides in some space, where in our applications, the points represent the locations of wireless nodes in the real world." Random counting measure, a more straightforward way of presenting a point process, can be used to define a point process mathematically as follows:

$$\Psi(B) = \Sigma_{X_i\in\Phi}\mathbb{1}\left(X_i \in B\right) \tag{2.6}$$

  where Φ is the point process, X_i represents the points in the point process, and B is a subset of the Euclidean space $\mathbb{R}^d$.

In the following subsections, some of the basic concepts of point processes are explained. Firstly, I start with the important measures of point processes, which are required for analyzing and deriving the important metrics of wireless mobile networks. Afterwards, some of the most suitable point processes for modeling wireless mobile networks and their characteristics are introduced.

2.3.1 Statistical Measures

In this section, two important measures, which are extensively being employed in a general point process, are introduced. Additionally, for more details about these measures, a passionate reader can refer to [34].

2.3.1.1 Mean Measure

The mean or expectation measure calculates the mean number of points in a point process. Mean measure can also be determined for lower subsets of a point process. For example, given that B is a subset of the point process Ψ, μ determines the average over all points in set B, i.e.,

$$\mu(B) = \mathbb{E}[\Psi(B)]. \tag{2.7}$$

2.3.1.2 Probability Generating Functional (PGFL)

The probability generating function (PGFL) is defined as:

$$M_{\Phi}(g) = \mathbb{E}\left[\prod_{X_i \in \Phi} g(X_i)\right]. \tag{2.8}$$

In other words, PGFL the expectation over the product of the value of a particular function at any point in a point process. Now assuming $g(X_i) = e^{-sf(X_i)}$, then the calculation of PGFL results in the Laplace transform of the function $g(\cdot)$. PGFL plays a significant role in many wireless networks, as it can be used to characterize interference which is a very important metric in almost all wireless applications.

2.3.2 Poisson Point Process

There are several types of point processes, which based on their mathematical characteristics, can be used for suitable wireless mobile communication networks. The most important point processes include the Poisson point process (PPP), Binomial point process (BPP), Matern point process (MPP), Cox point process (CPP), and the complete list of them can be found in [35]. PPP is the most straightforward and analytically tractable point process.

A point process is PPP with intensity measure Λ on Euclidean space $\mathbb{R}^{\mathrm{d}}$ such that

- *Given any compact set $B \subset \mathbb{R}^d$, the number of points for this set which is defined as $N(B)$ has a Poisson with expectation $\Lambda(B)$. Assuming $\Lambda = \lambda$, then*

$$\mathbb{P}\{N(B) = k\} = \exp\left(-\int \lambda(x)\, dx\right).\frac{(\lambda(x)\, dx)}{k!} \tag{2.9}$$

- *If all the sets B_1, B_2, ..., B_n are disjoint compact sets, then $N(B_1)$, $N(B_2)$, ..., $N(B_n)$ are independent.*

A particular case of PPP is homogeneous PPP, where $\Lambda(B) = \lambda|B|$. Further, stationary and motion-invariant point processes are two special cases of PPP. If the distribution of a PPP is invariant to translation, then the PPP is stationary, and a PPP is motion-invariant if the distribution of the point process is invariant to rotations regarding the origin [33]. An example of a PPP is presented in Fig. 2.1.

2.3.3 Binomial Point Process

If a fixed number of points is identically and independently distributed on a compact $W \subset \mathbb{R}^d$, then the result is Binomial Point Process (BPP). Moreover, the points in a

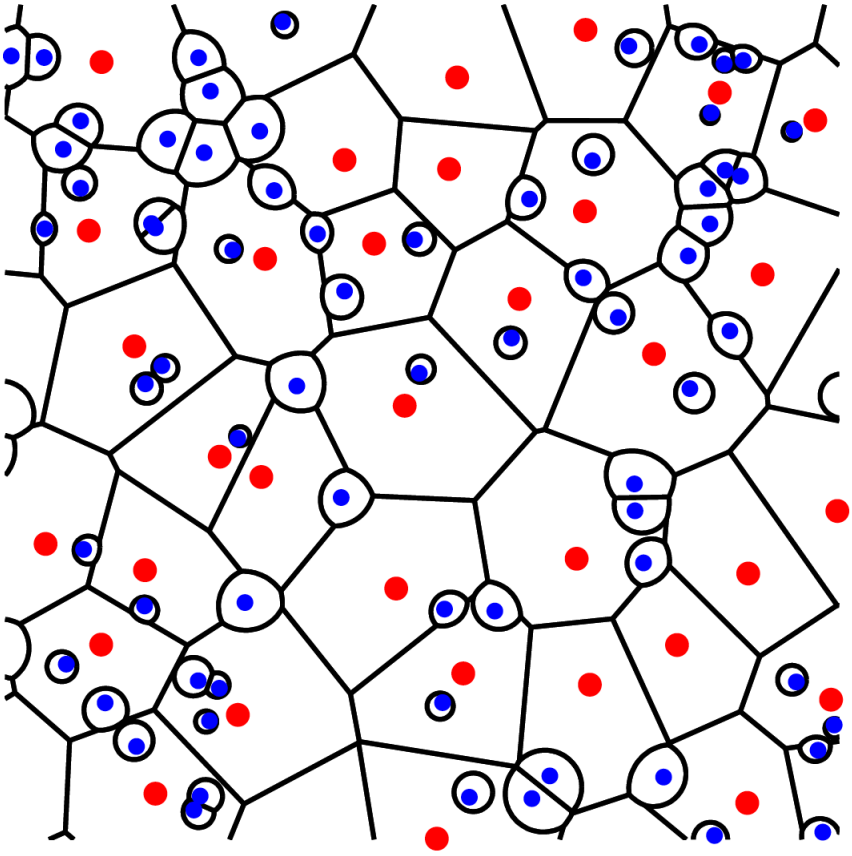

Figure 2.1: A PPP for two tier networks [2]. $\frac{points}{m^2}$

subset $A \subset W$ binomially distributed with parameters $n = \Psi(W)$ and $p = \frac{|A|}{|W|}$, and the intensity of points is as follows:

$$\Lambda(A) = n\frac{|A \cap W|}{|W|} \tag{2.10}$$

This kind of PP is suitable for modeling a wireless network in which there are a fixed number of BSs in a finite wireless network area. An example of such a network is sensor nodes in a parking lot to monitor vehicles that move in and out. [36, 37].

2.3.4 Hard-core Point Processes

In a hard-core Point processes (HCPP), the distance between two points is more than a predefined hard core distance $\delta > 0$. In another words, the set $\psi = \{x_i; i = 1, 2, 3, \cdots\}$ is HCPP, if $||x_i - x - k|| > \delta$, $\forall x_i, x_k \in \psi$, $i \neq k$.

This kind of PP is beneficial for modeling networks in which the BSs need to be separated by a minimum distance due reasons such as physical geographical constraints and network planning.

2.3.5 Matern Point Process

Matern Point Process is a kind of HCPP which is useful for modeling the spatial locations of BSs in wireless networks where the carrier sense multiple access (CSMA) MAC algorithm is applied. There are two kinds of Matern HCPP, both of which are produced based on a PPP. In the first one, all points within the proximity of the hard core distance δ are eliminated Fig. 2.2. Nonetheless, in the latter one, all the points are associated with a random mark, that is, $t \in [0, 1]$, and the thinning process will be performed only and only if there is another BS within distance δ with a smaller mark point($t = 0$).

2.4 Gil-Pelaez Inversion Theorem

The cumulative density function (CDF) of the SINR has an extensive application in wireless networks; for instance in calculating the outage and coverage probability of a typical user. Yet, sometimes it is undeniably tough to extract the CDF of SINR which is composed of the algebraic manipulation of several random variables (especially in large-scale networks). Fortunately, a theorem, also known as Gil-Pelaez inversion

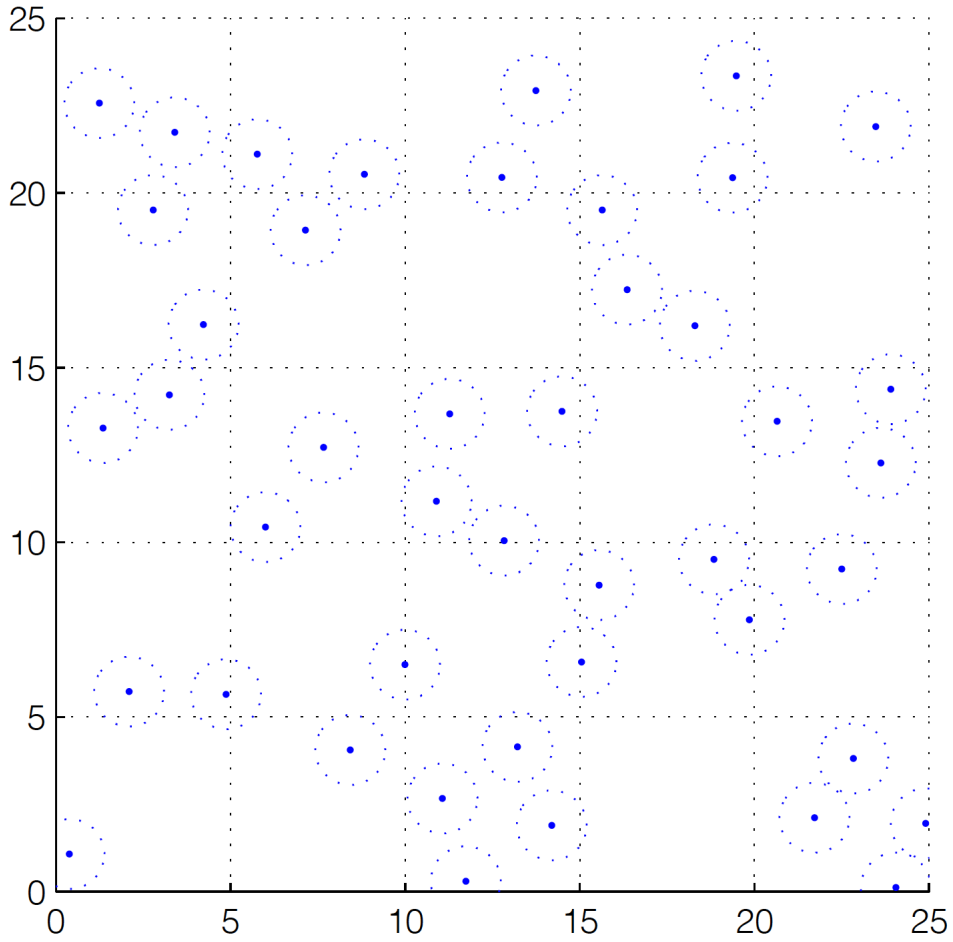

Figure 2.2: Type I of Matern HCPP, and this sequence of points are generated from the PPP in Fig. 2.1 and hard core distance $\delta = 2m$.

theorem, makes it possible to compute the CDF of the SINR using characteristic functions (related to the Laplace Transforms or Moment generating functions of the random variables).

If $F(x)$ is a one-dimensional cumulative distribution function (CDF),then its equivalent characteristic function, which is a complex function of real varibale t is:

$$\Omega(t) = \int_{-\infty}^{\infty} e^{itx} dF(x). \tag{2.11}$$

Now, according to the inversion version theorem, the CDF can be calculated as follows

$$F(x) - F(0) = \frac{1}{2\pi} \int_{-\infty}^{\infty} \frac{1 - e^{-itx}}{it} \Omega(t) dt. \tag{2.12}$$

In some cases, calculating the constant $F(0)$ is significantly troublesome, yet there is another version of this theorem which obviates the need for computation of $F(0)$. The CDF of RV x given its corresponding characteristic function $\Omega(t)$ is

$$F(x) = \frac{1}{2} - \frac{1}{2\pi} \int_{-\infty}^{\infty} \frac{\mathrm{Im}\left[e^{-tx}\Omega\left(t\right)\right]}{t} dt. \tag{2.13}$$

2.5 Literature Review

To date, most of the research works considered analyzing the performance of a given THz transmission link [11] or THz-only network [27, 38]. For instance, the authors in [11] derived a closed-form expression of the outage probability and ergodic capacity considering a THz wireless fiber extender system (i.e., a single transmission link) with ideal and non-ideal RF front-end. Using tools from stochastic geometry and considering interference-limited regime, the authors derived the mean interference in a THz-only network [27]. However, the closed-form expression of the mean interference was neither applicable for a general case, nor the expression was applied to the outage analysis. Instead, the authors approximate the distribution of the interference with log-logistic distribution to overcome the intractable outage calculation. Nevertheless, as the authors mentioned, the use of log-logistic approximation might not be

Table 2.1: Existing State-of-the-Art in Interference Analysis and Performance Modeling in THz Networks

Reference	**Interference Model**	**Research Gaps**	**LoS/NLoS**
[11]	NA	Single THz link	LoS
[27]	Mean Interference	No closed form solution for interference	LoS
[38]	Approximated with normal distribution	Interference Approximation and coverage probability	LoS
[39]	Mean interference	Interference Approximation and coverage probability	LoS
[40]	No exact closed-form solution for interference	Hybrid RF/THz deployment on each BS	LoS/NLoS

accurate in all scenarios. In [38], the authors analyzed the reliability and end-to-end latency considering a THz-only network with a finite number of BSs. The interference distribution was approximated with a normal distribution. In [39], the interference and outage probability in a THz-only network was investigated. The interference was approximated with mean interference. The authors in [40] derived the approximate coverage probability in a single-tier network, where BSs can use either RF or THz. Indoor THz communication is factored in in terms of achievable as well as coverage probability in [41]. The summary the works in this litrature is provided in **Table 2.1**.

2.6 Summary

In this section, an overview of the progress in wireless mobile networks got presented. We saw that the evolution of mobile networks' requirements has made it indisputable to migrate to the higher frequencies. I presented the challenges as to move to the

higher frequencies, and we saw that there is a requirement for a mathematical framework to capture the characteristics of THz band, and provide exact analytical results for the investigation of such networks. In the following chapter, my considered system model and the analysis of it are provided.

Chapter 3

Coverage Analysis in Coexisting RF/THz Network

3.1 Contributions

To my best knowledge, none of the research works presented a comprehensive analytic framework to characterize the exact interference statistics and coverage probability of users in a THz-only network or a coexisting two-tier RF and dense THz network (i.e., where the intensity of TBSs can be significantly high compared to the conventional RF SBSs.

Using stochastic geometry, this thesis characterizes the statistics of the downlink interference and rate coverage probability of a typical user in a coexisting RF/THz network. The proposed framework can be customized for various network configurations, including (i) *THz-only* network where only TBSs exist and users associate to their nearest BS, (ii) *opportunistic RF/THz* network where a user associates to the BS with maximum biased received signal power (BRSP)[1], and (iii) *Hybrid* network where a user associates to both nearest RF and TBSs. I first characterize the exact

[1]BRSP-based association is considered by 3GPP in Release 10, where the users' power received from small SBSs has been artificially increased by adding a bias in order to avoid under-utilization of SBSs [42].

Laplace Transform (LT) of the aggregate interference and coverage probability of a user in a *THz-only* network. Then, I derive the coverage probability of a typical user in a *coexisting network*. Asymptotic approximations are presented for the large intensity of TBSs or small molecular absorption coefficients. Numerical results show the significance of BRSP over conventional reference signal received power (RSRP) association in a coexisting network and validate the derived expressions.

The rest of this chapter is organized as follows. The system model and its assumptions are explained in Section II. In Section III, the SG based model for interference is derived, and the closed-form formula for the Laplace transform of interference is calculated. In addition, in this section, the Laplace transform of interference is leveraged to calculate the coverage probability. The simulation and numerical results are provided and compared in Section IV to confirm the validity of the achieved derivations. Finally, in section V, the conclusion is provided.

3.2 System model and Assumptions

Consider a two-tier downlink network composed of RF SBSs and TBSs as well as users' devices. The locations of the conventional RF SBSs and TBSs are modeled as a two-dimensional (2D) homogeneous Poisson point processes (PPP) $\mathbf{\Phi}_R$ and $\mathbf{\Phi}_T$ with intensities λ_R and λ_T, respectively. The locations of the users follow independent homogeneous PPP $\mathbf{\Phi}_u$ with intensity λ_u.

Each user measures the channel quality from each BS and then associate to the chosen BS according to a predefined association mechanism. It is important to note that user association can be performed based on both the instantaneous received power [43, 44] and maximum long-term averaged received power [45–49]. This is

because considering short-term fading can result in unnecessary handovers, that is, the "ping-pong effect". In order to circumvent this phenomenon, the received signal is averaged over the period of the measurement in LTE. This assumption, also has been considered in other research works [46–49] and is considered as more realistic compared to instantaneous received power based user association [49, page1]. The BSs serve associated users in orthogonal time slots or channels. I consider the performance of a typical user who is located at the origin.

3.2.1 RF Channel and SINR Model

The RF channel experiences both the channel fading and path-loss. Thus, the received signal power at the typical user can be modeled as $h(\rho) = \gamma_R \rho^{-\alpha} \chi$, where $\gamma_R = \frac{c^2}{(4\pi f_R)^2}$, χ is the exponentially distributed channel power with unit mean from the tagged SBS, α is the path-loss exponent, ρ is the distance of the typical user to the serving SBS, f_R is the RF carrier frequency in GHz, and $c = 3 \times 10^8$ m/s is the speed of light. I consider SBSs equipped with omni-directional antennas. Therefore, the signal-to-interference-plus noise ratio (SINR) of a typical user on RF transmission channel can be modeled as:

$$\mathrm{SINR}_R = \frac{P_R \gamma_R \rho_0^{-\alpha} \chi_0}{N_0^R + I_{\mathrm{agg}}^R}, \tag{3.1}$$

where χ_0 is the fading channel gain of the typical user from the desired SBS, P_R is the transmit power of the SBSs, N_0^R is the thermal noise at the receiver, $I_{\mathrm{agg}}^R = \sum_{i \in \Phi_R \setminus 0} P_R \gamma_R \rho_i^{-\alpha} \chi_i$ is the aggregate interference at the typical user from the interfering SBSs, ρ_i is the distance between the i-th interfering SBS and the typical user, and χ_i is the fading channel gain from the i-th interfering SBS.

3.2.2 THz Channel and SINR Model

Due to the high molecular absorption and the dense deployment, the LoS transmissions are dominant than the NLoS transmissions. Therefore, in this chapter, following [24,27,38,50]. I model the line-of-sight (LoS) channel propagation[2] between users and TBSs as $h\left(r\right)=\frac{c^{2}}{\left(4\pi f_{T}\right)^{2}}\frac{\exp(-k_{a}(f)r)}{r^{2}}$, where $k_{a}\left(f\right)$ is the molecular absorption coefficient, r is the distance between the transmitter and receiver, f_{T} is the operating THz frequency, c is the speed of light, and $G_{\mathrm{tx}}^{\mathrm{T}}\left(\theta\right)$ as well as $G_{\mathrm{rx}}^{\mathrm{T}}\left(\theta\right)$ are the directional transmitter and receiver antenna gains, respectively. The directional antennas are modeled as [51]:

$$G_{q}^{T}\left(\theta\right)=\begin{cases}G_{q}^{(\max)} & \mid\theta\mid\leq w_{q}\\ G_{q}^{(\min)} & \mid\theta\mid>w_{q}\end{cases}, \tag{3.2}$$

where $q\in\{\mathrm{tx},\mathrm{rx}\}$, $\theta\in[-\pi,\pi)$ is the angle of the boresight direction, w_{q} is the main lobe beamwidth, $G_{q}^{(\max)}$ and $G_{q}^{(\min)}$ are beamforming gains of the main and side lobes, respectively. The typical user and its desired TBS align such that their main lobes coincide through beam alignment techniques. The alignment beten the typical user and an interferer is defined as a random variable D, which can take values in $\{G_{\mathrm{tx}}^{(\max)}G_{\mathrm{rx}}^{(\max)},G_{\mathrm{tx}}^{(\max)}G_{\mathrm{rx}}^{(\min)},G_{\mathrm{tx}}^{(\min)}G_{\mathrm{rx}}^{(\max)},G_{\mathrm{tx}}^{(\min)}G_{\mathrm{rx}}^{(\min)}\}$, and the corresponding probability for each case is $F_{\mathrm{tx}}F_{\mathrm{rx}}$, $F_{\mathrm{tx}}(1-F_{\mathrm{rx}})$, $(1-F_{\mathrm{tx}})F_{\mathrm{rx}}$, and $(1-F_{\mathrm{tx}})(1-F_{\mathrm{rx}})$, where $F_{\mathrm{tx}}=\frac{\theta_{\mathrm{tx}}}{2\pi}$ and $F_{\mathrm{rx}}=\frac{\theta_{\mathrm{rx}}}{2\pi}$, respectively. Assuming that the main lobe typical user's receiver is coinciding with that of its desired TBS, its SINR the can be formulated as follows:

$$\mathrm{SINR}_{T}=\frac{P_{\mathrm{T}}G_{\mathrm{tx}}^{(\max)}\left(\theta\right)G_{\mathrm{rx}}^{(\max)}\left(\theta\right)\frac{c^{2}}{\left(4\pi f_{T}\right)^{2}}\frac{\exp(-k_{a}(f)r)}{r^{2}}}{N_{0}^{T}+I_{\mathrm{agg}}^{T}}, \tag{3.3}$$

[2]The consideration of NLoS with accurate reflection, scattering, and diffraction models deserves a separate study and has been left for future investigation.

where $I_{\text{agg}}^{T} = \sum_{\text{i}\in\Phi_T\setminus 0} P_{\text{T}} D_i h\left(r_i\right)$ is the aggregate interference at the typical user by their maximum gain, r_i is the distance of the typical user to the interfering TBSs. For brevity, define $\gamma_T = G_{\text{tx}}^{(\max)}\left(\theta\right) G_{\text{rx}}^{(\max)}\left(\theta\right) \frac{c^2}{\left(4\pi f_T\right)^2}$. assume that the interferers' main lobe coincides with the users' main lobe[3] with the probability of $F = F_{\text{tx}} F_{\text{rx}}$, and thus, $D = G_{\text{tx}}^{(\max)}\left(\theta\right) G_{\text{rx}}^{(\max)}\left(\theta\right)$. Also, P_T is the transmit power of the TBSs, and N_0^T denotes the thermal noise and the noise resulted from the molecular absorption.

3.3 Coverage Probability in THz-Only Network

In this section, I derive the LT of the aggregate interference and the coverage probability experienced by a typical user in a THz-only network with the nearest BS association.

Lemma 1. *Conditioned on the distance of a typical user from the serving TBS, the LT of the aggregate interference, at a typical device in THz network, can be derived as follows:*

$$\mathcal{L}_{I_{\text{agg}}^{T}|r}(s) = \exp\left(2\pi\lambda_T \sum_{l=1}^{\infty} \frac{\left(-s\gamma_T F P_{\text{T}}\right)^l \Gamma\left(2-2l, l k_a\left(f\right) r\right))}{\left(l k_a\left(f\right)\right)^{2-2l} l!}\right).$$

Proof. See **Appendix A**. □

Define the rate coverage probability as the probability with which a typical user achieves the desired target rate of R_{th}. Subsequently, using $R_{\text{th}} = W_T \log_2(1+\text{SINR})$ (where W_T is the THz transmission bandwidth), the desired SINR threshold of a typical user can be calculated as $\tau_T = 2^{\frac{R_{\text{th}}}{W_T}} - 1$. The rate coverage probability can

[3]For simplicity, I consider negligible side lobe gains. However, the framework can be extended by averaging over variable D and considering all four possible interference components in $I_{\text{agg}}^{\text{T}}$ with different antenna gains. These four interference variables are independent and their LTs can be given using **Lemma 1**. $\mathcal{L}_{I_{\text{agg}}^{T}|r}(s)$ can thus be given as the product of the LTs.

thus be given as follows:

$$\mathcal{P}_T = \Pr\left(\mathrm{SINR}_T > 2^{\frac{R_{\mathrm{th}}}{W_T}} - 1\right) = \Pr\left(\mathrm{SINR}_T > \tau_T\right). \tag{3.4}$$

Taking the desired signal power at the typical user $S(r) = P_T \gamma_T \frac{\exp(-k_a(f)r)}{r^2}$ and using the Gil-Pelaez inversion theorem [52], $\mathcal{P}_T$ can be derived as follows:

$$\begin{aligned}\mathcal{P}_T &= \Pr\left(\frac{S(r)}{N_0^T + I_{\mathrm{agg}}^T} > \tau_T\right) = \Pr\left(S(r) > \tau_T I_{\mathrm{agg}}^T + \tau_T N_0^T\right), \\ &= \frac{1}{2} - \frac{1}{\pi}\int_0^\infty \frac{\mathrm{Im}[\phi_\Omega(\omega)]}{\omega} e^{-\tau_T N_0^T}\, d\omega, \end{aligned} \tag{3.5}$$

where $\Omega = S(r) - \tau_T I_{\mathrm{agg}}^T$, $\phi_\Omega(w) = \mathbb{E}[e^{-j\omega\Omega}]$ is the characteristic function (CF) of Ω, $\mathrm{Im}(\cdot)$ is the imaginary part of $\phi_\Omega(\cdot)$. Note that $\phi_\Omega(\omega)$ can be computed as follows:

$$\phi_\Omega(\omega) = \mathbb{E}_r\left[\phi_{\Omega|r}(\omega)\right] = \mathbb{E}_r[e^{-j\omega S(r)} \mathcal{L}_{I_{\mathrm{agg}}^T|r}(-j\omega\tau_T)],$$

where $\mathcal{L}_{I_{\mathrm{agg}}^T|r}$ is given in **Lemma 1**.

3.4 Coverage in Coexisting RF/THz Network

In the coexisting network, the user can either associate to a given SBS or TBS based on the maximum BRSP with a probability termed as *association probability*.

Given the received powers from TBSs and SBSs as $P_r^{\mathrm{THz}} = P_T \gamma_T \times \frac{\exp(-k_a(f)r)}{r^2}$ and $P_r^{\mathrm{RF}} = P_R \gamma_R \times \rho^{-\alpha}$, respectively, the probability of association with TBS can be

derived as follows:

$$\begin{aligned}\mathcal{P}_{A_T} &= \mathbb{E}_r\left[\Pr\left[B_T P_r^{\mathrm{THz}} > P_r^{\mathrm{RF}}\right]\right], \\ &= \mathbb{E}_r\left[\Pr\left[P_T B_T \gamma_T \frac{\exp\left(-k_a\left(f\right) r\right)}{r^2} > P_R \gamma_R \rho^{-\alpha}\right]\right], \\ &\overset{(a)}{=} \mathbb{E}_r\left[\exp\left(-\pi\lambda_R\left(K r^2 \exp\left(k_a\left(f\right) r\right)\right)^{\frac{2}{\alpha}}\right)\right],\end{aligned} \tag{3.6}$$

where $K = \frac{P_R \gamma_R}{B_T P_T \gamma_T}$, $B_T > 1$ is the bias value to encourage association with THz layer, $0 \leq B_T < 1$ encourages association to RF layer, $B_T = 1$ yields conventional RSRP and (a) follows from the null property of PPP Φ_R. This property implies that given a tier of RF SBSs with intensity λ_{R}, the probability that no RF BSs are closer to typical user than the distance z is $\mathbb{P}\left[\rho \geq z\right] = \exp\left(-\pi\lambda_R z^2\right)$.

Taking the expectation, the association probability of a typical user to TBSs can be derived as in the following lemma.

Lemma 2. *Given that the user associates with the layer that provides the maximum BRSP, the probability of association to the THz layer is given as follows:*

$$\mathcal{P}_{A_T} = \sum_{j=0}^{\infty} \frac{(-1)^j \Gamma\left[v_j\right] \delta_{T,j}}{\left(2\beta_T\right)^{\frac{v_j}{2}} j!} \exp\left(\frac{-\eta_j}{8\beta_T}\right) D_{-v_j}\left(\frac{-\eta_j}{\sqrt{2\beta_T}}\right),$$

where $\beta_T = \pi\lambda_T$, $\delta_{T,j} = 2\pi\lambda_T\left(\pi\lambda_R K^{\frac{2}{\alpha}}\right)^j$, $\nu_j = \frac{4j}{\alpha} + 2$, $\eta_j = -\frac{2jk(f)}{\alpha}$, *and* $D_\nu\left(z\right)$ *is the parabolic cylinder function (PCF) ([53], Eq. 9.240). Clearly, the probability that a device associates to the RF layer is given by*

$$\mathcal{P}_{\mathrm{A_R}} = 1 - \mathcal{P}_{\mathrm{A_T}}. \tag{3.7}$$

Proof. See **Appendix B**. □

As the future networks will be highly dense, the density of TBSs can be very high ($\lambda_T \to \infty$). In addition, for indoor applications [38], the absorption loss can approach zero ($k_a(f) \to 0$). By demonstrating the limit of ∞, mean that the intensity can be quite large (which may not necessarily be close to ∞) and this scenario may or may not happen in practice. In both special cases, the association probability can be simplified as follows.

Corollary 1. *When $\lambda_T \to \infty \Longrightarrow z \to 0$ and $k_a \to 0 \Longrightarrow z \to 0$, the argument of $D_\nu(z)$ in Lemma 2 tends to zero. For $z = 0$, $D_\nu(z)$ will be simplified to $\frac{\sqrt{\pi}}{2^{\frac{1}{2}b+\frac{1}{4}}\Gamma\left(\frac{3}{4}+\frac{1}{2}b\right)}$, where $b = -\frac{1}{2} - \nu$ and $\Gamma(z)$ is the gamma function ([53], Eq. 8.31). As a result, $\mathcal{P}_{\mathrm{A_T}}$ in lemma 2 can be simplified as follows:*

$$\mathcal{P}_{\mathrm{A_T}} = \sum_{j=0}^{\infty} \frac{\sqrt{\pi}\,(-1)^j\,\delta_j\,(2\beta)^{-\frac{v_j}{2}}\,\Gamma\left[v_j\right]}{2^{\frac{1}{2}b_j+\frac{1}{4}}\Gamma\left(\frac{3}{4}+\frac{1}{2}b_j\right)j!} \exp\left(\frac{-\eta_j}{8\beta}\right), \tag{3.8}$$

where $b_j = -\frac{1}{2} - \nu_j$.

Since a typical user can associate with either RF or THz layer, the total coverage probability can be calculated as:

$$\mathbb{C} = \mathcal{P}_{\mathrm{A_T}}\mathbb{P}_{C_{\mathrm{T}}} + \mathcal{P}_{\mathrm{A_R}}\mathbb{P}_{\mathcal{C}_{\mathrm{R}}}, \tag{3.9}$$

where $\mathcal{P}_{\mathrm{A_T}}$ and $\mathcal{P}_{\mathrm{A_R}}$ are defined in **Lemma 2**. Also, $\mathbb{P}_{\mathrm{C_T}}$ and $\mathbb{P}_{C_{\mathrm{R}}}$ refer to the coverage probability conditioned that the typical user associates to a given TBS and RF SBS, respectively. Since the TBSs and RF SBSs are distributed according to different PPPs, the distance of a typical user to its serving BS depends on the tier to which the user is associated. Subsequently, the distribution of the distance of the typical user to its serving BS in k-th tier can be given as:

Lemma 3. *The distribution of the distance of a typical user if it is tagged to the THz layer and SBS layer can be given, respectively, as follows:*

$$f_{\hat{X}_T}(\hat{x}) = \frac{2\pi\lambda_T\hat{x}}{\mathcal{P}_{\mathrm{A_T}}} \exp\left(-\pi\lambda_R(K\hat{x}^2)^{2/\alpha}e^{2k_a(f)\hat{x}/\alpha} - \pi\lambda_T\hat{x}^2\right),$$

$$f_{\hat{X}_R}(\hat{x}) \approx \frac{2\pi\lambda_R\hat{x}}{\mathcal{P}_{\mathrm{A_R}}} \exp\left(-\pi\lambda_T\left(\frac{K\hat{x}^\alpha}{\pi}\right)^{\frac{1}{2+\mu}} - \pi\lambda_R\hat{x}^2\right),$$

where μ is a factor defined in the proof.

Proof. See **Appendix C**. □

Lemma 4. *The calculation of $\mathbb{P}_{\mathrm{C_T}}$ can be performed using the Gil-Pelaez inversion theorem as given in* (3.14) *where*

$$\phi_\Omega(\omega) = \mathbb{E}_{\hat{X}_T}\left[\phi_{\Omega|\hat{X}_T}(\omega)\right] = \mathbb{E}_{\hat{X}_T}\left[e^{-j\omega S(\hat{x})}\mathcal{L}_{I^T_{\mathrm{agg}}|\hat{X}_T}(-j\omega\tau_T)\right],$$

and the PDF of $\hat{X}_T$ is given in ***Lemma 3****. Considering the interference limited regime, the conditional coverage probability of the user when associated to RF layer can be given as:*

$$\begin{aligned}\mathbb{P}_{C_{\mathrm{R}}} &= \Pr\left[\chi_0 > \tau_R P_R^{-1}\gamma_R^{-1}\hat{x}^\alpha I^R_{agg}\right],\\ &= \mathbb{E}_{I^R_{agg},\hat{x}}\left[\exp(-\tau_R P_R^{-1}\gamma_R^{-1}\hat{x}^\alpha I^R_{agg})\right], \\ &= \int_0^\infty \mathcal{L}_{I^R_{agg}}(\tau_R P_R^{-1}\gamma_R^{-1}\hat{x}^\alpha) f_{\hat{X}_R}(\hat{x})\, d\hat{x},\end{aligned} \tag{3.10}$$

where $\mathcal{L}_{I^R_{agg}}\left(\tau_R P_R^{-1}\gamma_R^{-1}\hat{x}^\alpha\right) = \exp\left(-\pi\hat{x}^2\lambda_R\mathcal{Z}(\tau_R,\alpha)\right)$, $\mathcal{Z}(\tau_R,\alpha) = \frac{2\tau_R}{\alpha-2}{}_2F_1[1, 1-\frac{2}{\alpha}; 2-\frac{2}{\alpha}; -\tau_R]$, and ${}_2F_1[\cdot]$ is Gauss Hypergeometric function [53].

Remark 1. *The coverage probability of the hybrid RF/THz scheme can be given as $\mathbb{C}_{\mathrm{Hybrid}} = 1 - (1-\mathcal{P}_T)(1-\mathcal{P}_R)$, where $\mathcal{P}_T$ is given in Eq. (3.14),*

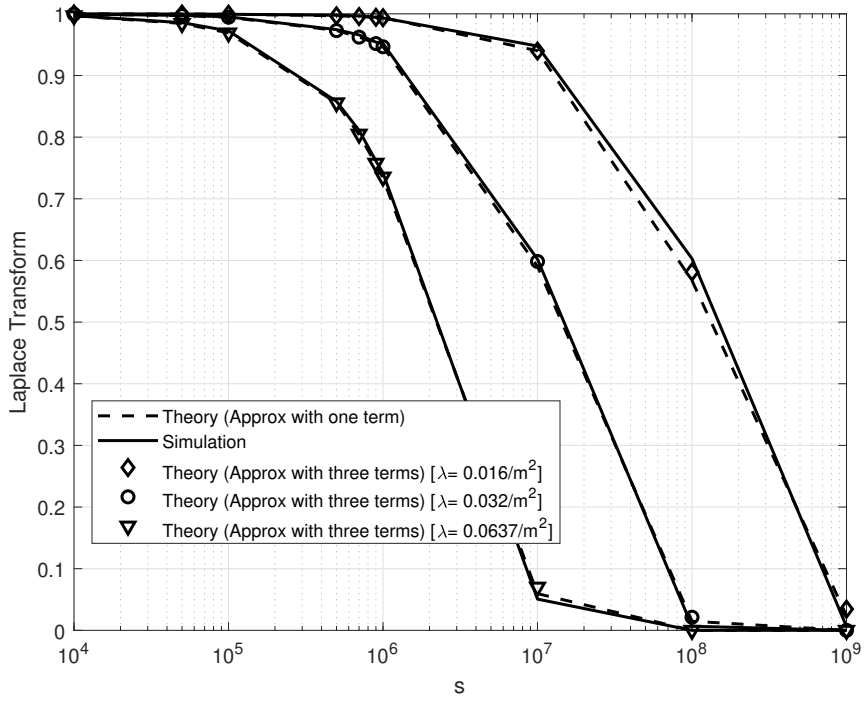

Figure 3.1: LT of the aggregate interference as a function of the intensity of TBSs, $k_a(f) = 0.05$, f =1.0 THz.

$\mathcal{P}_R = 2\pi\lambda_R \int_0^\infty \rho \mathcal{L}_{I_{agg}^R}(\tau_R P_R^{-1} \gamma_R^{-1} \rho^\alpha) \exp(-\pi\lambda_R \rho^2) d\rho$ *is the coverage probability of the RF-only network and* $\mathcal{L}_{I_{agg}^R}(\cdot)$ *is given in* **Lemma 4**.

3.5 Numerical Results and Discussions

Unless stated otherwise, the simulation parameters are listed herein. Users are distributed within a circular disc of radius 100 m. The antenna gains of TBSs G_{tx}^T and G_{rx}^T are set as 25 dB. The transmit powers of TBSs and RF SBSs are 1 W. Three values for $k_a(f)$ are considered, i.e., 0.05, 0.1, and 0.2 m^{-1} with 1% of water vapor molecules. These absorption values are chosen from the realistic database and

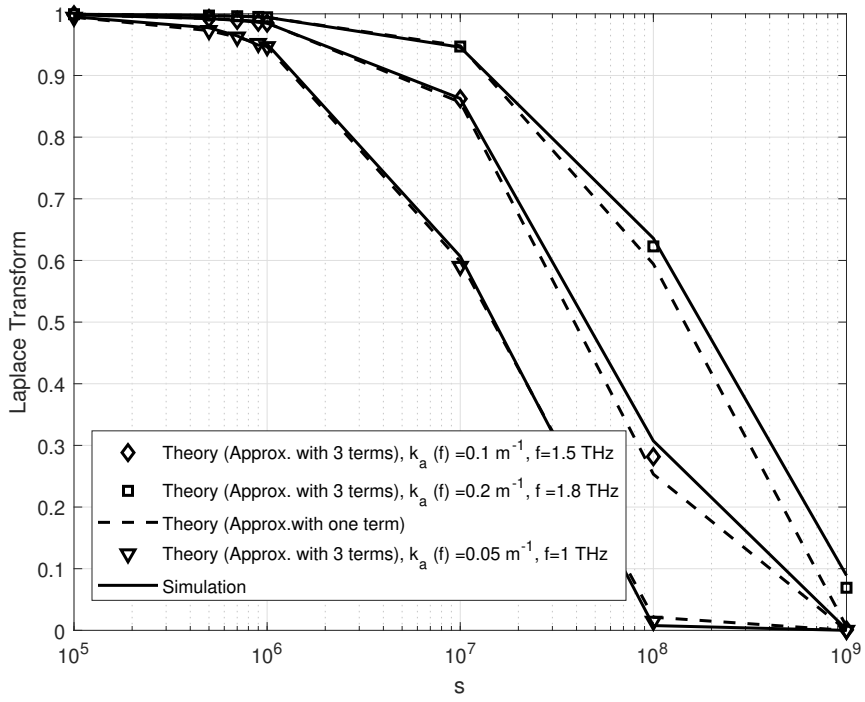

Figure 3.2: LT of the aggregate interference as a function of the molecular absorption coefficients, $\lambda_T = 0.032$ per m^2.

their corresponding central frequencies are 1.0 THz, 1.5 THz, and 1.8 THz, respectively [23] [54]. The desired rate threshold is taken as 5 Gbps. The RF transmission frequency is set as 2.1 GHz and α=2.5. The RF and THz transmission bandwidths are set as 40 MHz and 0.5 GHz, respectively. The intensity of RF SBS λ_R is set as 0.0001 BSs/m^2.

Fig. 3.1 depicts the LT of the aggregate interference at the typical user (averaged over a large number of realizations of the desired link distance r). As the LT of aggregate interference can be used to compute all moments of the aggregate interference, Fig. 3.1 and Fig. 3.2 are shown to evaluate the accuracy of the LT of $I_{\mathrm{agg}}^{\mathrm{T}}$. The theoretic results are calculated by taking the first three terms as well as only one

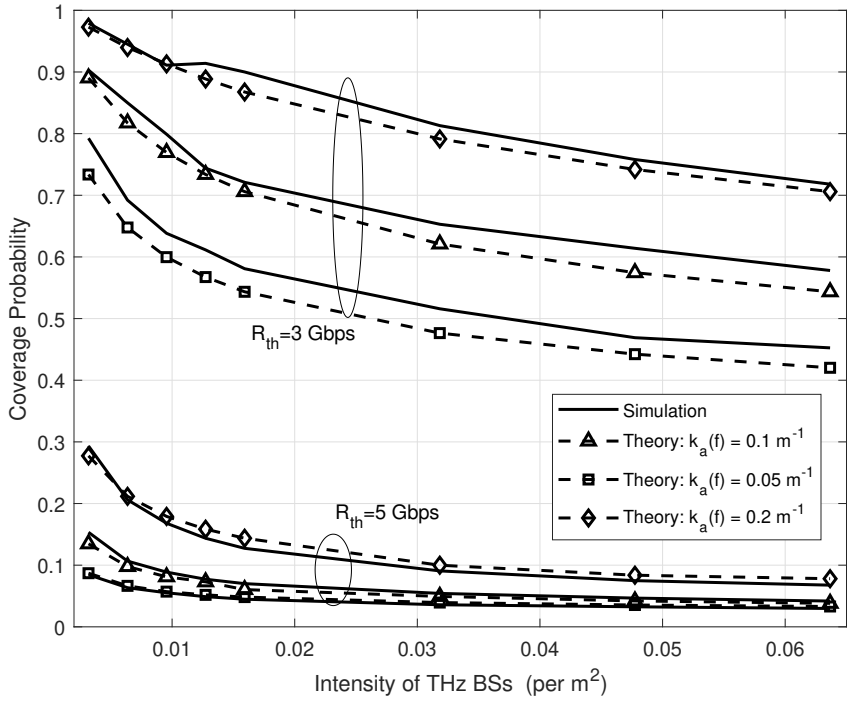

Figure 3.3: Coverage probability of a user in THz-only network.

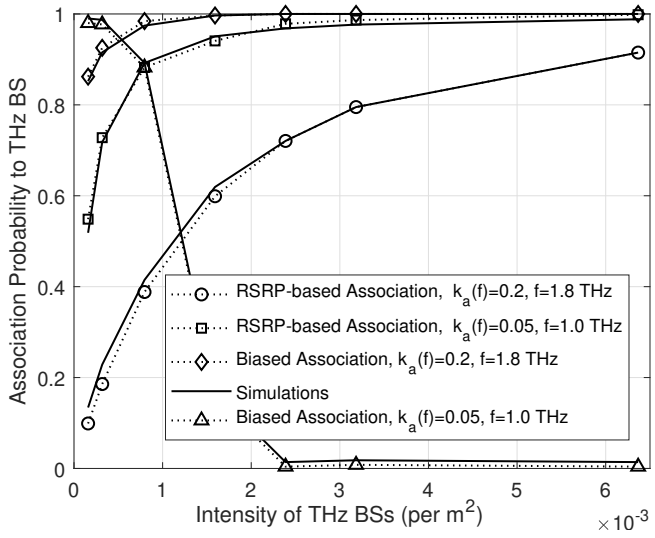

Figure 3.4: Association probability as a function of the intensity of TBSs, $k_a(f) = 0.2$ m^{-1}, f =1.8 THz, G_T^T and $G_R^T = 15$ dB, α=3.6.

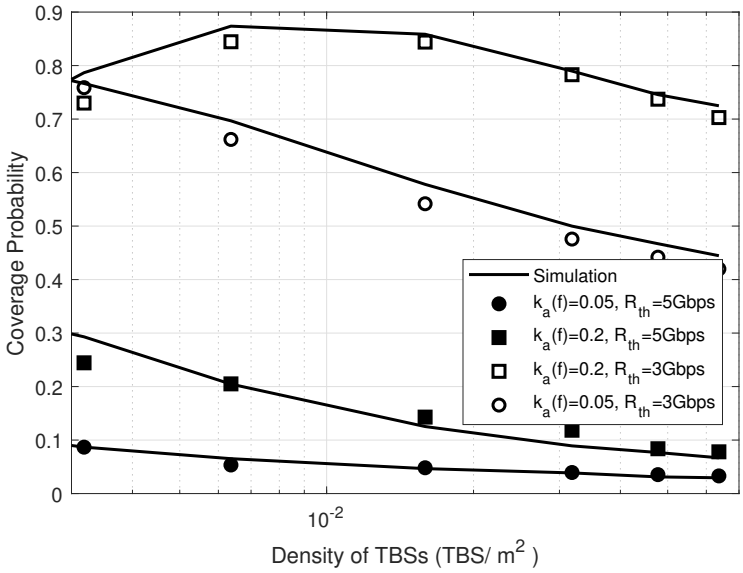

Figure 3.5: Coverage probability in coexisting network, $\lambda_T = 0.1$ m^{-2}. (c) Coverage probability of a typical user in THz-only network, $k_a(f) = 0.05\text{m}^{-1}$, B=$[10^3, 10^2, 1, 10^{-3}, 10^{-4}, 10^{-4}, 10^{-5}]$.

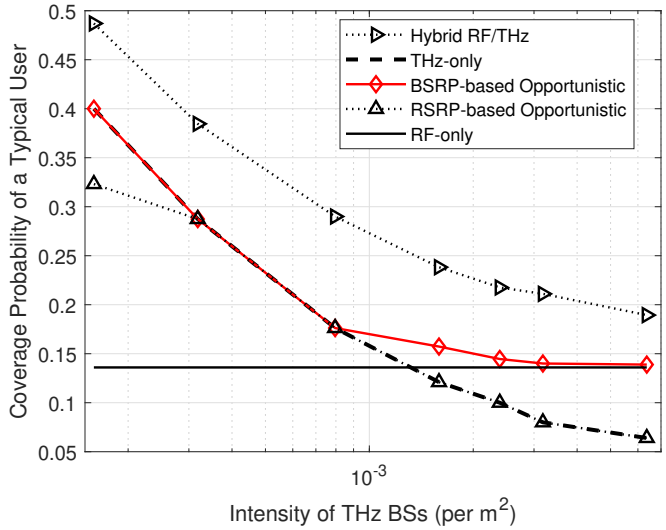

Figure 3.6: Comparison of. the Coverage probability of a typical user in THz-only, RF-only, and hybrid RF/THz network, $k_a(f) = 0.05\text{m}^{-1}$.

term of the summation in **Lemma 1**. There is a close match between the theory and simulations. For a given s, increasing LT values mean that the aggregate interference is reducing and vice versa. In Fig. 3.1, for a given s, note that increasing the intensity of TBSs, LT decreases rapidly (which implies interference increases). Similarly, for a given s, note that increasing the $k_a(f)$ in Fig. 3.2, LT increases (which implies interference decreases due to lower absorption loss at the interfering links). The coverage probability of a user in a THz-only network is demonstrated in Fig. 3.3. The theoretical results (with the first three terms of the infinite summation) show a close match with the simulations. Note that by increasing the molecular absorption coefficient, the coverage probability increases. This is in agreement with our observations in Fig. 3.1 and 3.2 where the total interference reduces with increasing $k_a(f)$.

The association probability to the THz layer is depicted in Fig. 3.4 against the intensity of TBSs (λ_T). I consider B=[1000, 100, 1, 0.001, 0.0001, 0.0001, 0.00001] when $k_a(f) = 0.05\text{m}^{-1}$, and B=[$10^6, 10^5, 10^4, 10^4, 10^3, 10^3, 10^3$] when $k_a(f) = 0.2\text{m}^{-1}$ For the RSRP-based association, the probability of user association to the THz layer increases with λ_T. Hover, in BRSP, the bias factor B_T is obtained numerically to maximize the coverage probability. Note that optimal bias to TBSs decreases with the increase in λ_T (which implies increased THz interference). Also, bias reduction is steep for low $k_a(f)$ (implying higher interference), whereas the reduction in bias is gradual for high values of $k_a(f)$ (implying lower interference). Fig. 3.5 shows the coverage probability of the opportunistic RF/THz system with unit bias value. From Fig. 3.4, it is clear that the typical user is likely to associate to the THz layer when bias is unity. Therefore, the total coverage probability is dominated by the behavior of the THz layer and shows similar behavior as the THz-only network.

Fig. 3.6 compares the performance of the typical user in coexisting RF/THz network with THz-only, RF-only, and hybrid RF/THz networks considering B=$[10^3, 10^2, 1, 10^{-3}, 10^{-4}, 10^{-4}, 10^{-5}]$. Hybrid RF/THz network outperforms all networks, since the typical user simultaneously uses both THz and RF transmissions. That is, the additional coverage is at the expense of increased network resources. Coexisting RF/THz with BRSP-based association maximizes the coverage by dynamically adapting to the best tier (since the bias factors are chosen to maximize the coverage) and outperforms the RF-only and the THz-only schemes.

3.6 Blockage Consideration

In the system model, I have considered a dense THz network; therefore, the probability of blockage is relatively low.

Nevertheless, incorporating the impact of blockages is an interesting extension, especially with non-dense THz deployments. In the following, I describe how the framework can be extended to include the blockages similar to the approach provided in [15].

The blocking phenomenon can be modeled as a thinning process where the transmissions from a specific number of BSs are considered as blocked. Subsequently, the intensity of the BSs gets reduced. Similar to [15], a Boolean blockage model in which obstacles are rectangles and are distributed following a homogeneous PPP of density λ_B. The rectangles length (L_k) and width (W_k) are independent and identically distributed, and their probability density functions are $f_L(x)$ and $f_W(x)$, respectively. The orientation of these rectangles is distributed uniformly in $[0, 2\pi)$. Then, according to [15], the number of blockages in a link of length r is a random variable with Poisson

distribution having mean $\xi r + p$, where $\xi = \frac{2\lambda_B(E\{W\}+E\{L\})}{\pi}$ and $p = \lambda_B E\{W\}E\{L\}$, where $0 < p < 1$ represents the area which is under blockages. Then, LOS probability $e^{[-(\xi r+p)]}$ (where ξ and p are constants) can be multiplied with $\Phi_\Omega|r(\omega)$ defined below **Equation 3.15** to accommodate the blockages. and the PDF of $\hat{X}_T$ is given in **Lemma 3**.

3.7 Side Lobe Gain Consideration for Antennas

In the system model, I have considered a consider negligible side lobe gains; therefore, yet incorporating the affect of antenna side lobe is straightforward.

I describe how the analytic framework can be extended to incorporate the impact of side lobes on the interference. As it is mentioned earlier, the antenna gain between the typical user and an interferer can be modeled as a random variable $D \in \{G_{\text{tx}}^{(\max)}G_{\text{rx}}^{(\max)}, G_{\text{tx}}^{(\max)}G_{\text{rx}}^{(\min)}, G_{\text{tx}}^{(\min)}G_{\text{rx}}^{(\max)}, G_{\text{tx}}^{(\min)}G_{\text{rx}}^{(\min)}\}$, and the corresponding probability for each value is $F_1 = F_{\text{tx}}F_{\text{rx}}$, $F_2 = F_{\text{tx}}(1 - F_{\text{rx}})$, $F_3 = (1 - F_{\text{tx}})F_{\text{rx}}$, and $F_4 = (1 - F_{\text{tx}})(1 - F_{\text{rx}})$, where $F_{\text{tx}} = \frac{\theta_{\text{tx}}}{2\pi}$ and $F_{\text{rx}} = \frac{\theta_{\text{rx}}}{2\pi}$, respectively. Now let us assume that the interference resulting from the side lobes is not negligible (i.e., side lobe gains are non-negligible). In this case, the SINR can be given as follows:

$$\text{SINR}_T = \frac{P_{\text{T}}G_{\text{tx}}^{(\max)}(\theta)\, G_{\text{rx}}^{(\max)}(\theta)\, \frac{c^2}{(4\pi f_T)^2}\frac{\exp(-k_a(f)r)}{r^2}}{N_0^T + I_{\text{agg}}^T}, \tag{3.11}$$

where $I_{\text{agg}}^T = \sum_{\text{i}\in\Phi_T\setminus 0} P_{\text{T}}D_i h(r_i)$. By averaging I_{agg}^T over D, it becomes:

$$I_{\text{agg}}^T = F_1 I_{\text{agg}}^1 + F_2 I_{\text{agg}}^2 + F_3 I_{\text{agg}}^3 + F_4 I_{\text{agg}}^4, \tag{3.12}$$

where,

$$
\begin{aligned}
I^1_{\text{agg}} &= \sum_{i\in\Phi_T\setminus 0} P_{\text{T}} G^{(\max)}_{\text{tx}} G^{(\max)}_{\text{rx}} h\left(r_i\right), \\
I^2_{\text{agg}} &= \sum_{i\in\Phi_T\setminus 0} P_{\text{T}} G^{(\max)}_{\text{tx}} G^{(\min)}_{\text{rx}} h\left(r_i\right), \\
I^3_{\text{agg}} &= \sum_{i\in\Phi_T\setminus 0} P_{\text{T}} G^{(\min)}_{\text{tx}} G^{(\max)}_{\text{rx}} h\left(r_i\right), \\
I^4_{\text{agg}} &= \sum_{i\in\Phi_T\setminus 0} P_{\text{T}} G^{(\min)}_{\text{tx}} G^{(\min)}_{\text{rx}} h\left(r_i\right),
\end{aligned}
\tag{3.13}
$$

The coverage probability can then be evaluated as given in the previous analysis by modifying $\Phi_\Omega(\cdot)$, i.e.,

$$
\mathcal{C}_T = \Pr\left(\frac{S(r)}{N_0^T + I^T_{\text{agg}}} > \tau_T\right) = \frac{1}{2} - \frac{1}{\pi}\int_0^\infty \frac{\text{Im}[\phi_\Omega(\omega)]}{\omega} e^{-\tau_T N_0^T} d\omega, \tag{3.14}
$$

where $\Omega = S(r) - \tau_T I^T_{\text{agg}}$ and then $\phi_\Omega\left(\omega\right)$ is calculated as follows:

$$
\phi_\Omega\left(\omega\right) = \mathbb{E}_r\left[\phi_{\Omega|r}\left(\omega\right)\right] = \mathbb{E}_r[e^{-j\omega S(r)}\mathcal{L}_{I^T_{\text{agg}}|r}\left(-j\omega\tau_T\right)], \tag{3.15}
$$

where $\mathcal{L}_{I^T_{\text{agg}}|r}$ can be given as follows:

$$
\begin{aligned}
\mathcal{L}_{I^T_{\text{agg}}}(s) &= \mathbb{E}_{\Phi_T}\left[e^{-sI^T_{\text{agg}}}\right] = \mathbb{E}_{\Phi_T}\left[e^{-s\sum_{i=1}^4 F_i I^i_{\text{agg}}}\right] \\
&\overset{(a)}{=} \prod_{i=1}^4 \mathbb{E}_{\Phi_T}\left[e^{-sI^i_{\text{agg}}}\right] = \prod_{i=1}^4 \mathcal{L}_{I^i_{\text{agg}}}(s),
\end{aligned}
\tag{3.16}
$$

where (a) follows from the fact that the Laplace Transform of the sum of independent random variables can be given by the product of their corresponding Laplace Transforms. Finally, the $\mathcal{L}_{I^i_{\text{agg}}}(s)$ can be given using **Lemma 1** by substituting appropriate

values of the probabilities F_i.

3.8 Summary

In this chapter, I first considered a system model, which comprised of THz and RF BSs. Then, I analyzed the performance of a typical user in THz-only network to evaluate the LT of the interference and coverage probability. Achieving exact analytical results, I continued with the analysis of the two-tier RF/THz network. Here, I first derived the user association probability considering BRSP-based association. Finally, I derive the coverage probability of a two-tier wireless cellular network operating at both RF and THz bands.

Chapter 4

Conclusions and Future Directions

In this chapter, I first provide a conclusion of this thesis. Then, I conclude this chapter by providing future research directions.

4.1 Conclusion

I presented a unified stochastic geometry framework to characterize the performance of a user in configurations such as RF-only, THz-only, opportunistic, and hybrid networks. Unlike previous works, closed-form and exact solutions are provided for LT of aggregate interference, association probability, and the distance distribution of a typical user to its tagged BS. The analytical results are verified through simulations. The opportunistic with BRSP scheme for association outperforms RF-only, THz-only, and opportunistic with the conventional RSRP-based association. For non-dense THz deployments, this work can be extended to include blockages using the approach in [15]. A Boolean blockage model can be considered where the number of blockages in a link are Poisson distributed. Then, LOS probability $e^{[-(\xi r+p)]}$ (where ξ and p are constants) can be multiplied with $\Phi_{\Omega}|r(\omega)$ to accommodate the blockages.

4.2 Future Work

There are some optimization issues in regard with the considered this system model yet to be answered. Also, there some challenges as to the use of THz in the other applications. Some of this concerns are as follows:

4.2.1 User Association with Machine Learning

The problem of handover prediction in such heterogeneous networks operating at well-explored bands; that is, RF, mm-Wave, VLC, and to name be three is addressed well by previous works. However, as the behavior of THz band is totally different from those band, the traditional and even recent proposed handover algorithms do not suit THz-only networks, not mention the co-existing RF/THz networks. Therefore, it is required to design new algorithms, capturing the characteristics of THz band, for user association within the layers - THz and RF, and between the layers.

4.2.2 Load-Aware Association and Scheduling in RF and THz Layer

Although THz is providing an ample of spectrum, RF has its distinguished feature, making it proper for some applications. Thus, it is more rational to associate users to each layer based on their need. One way to take apart users is to separate them based on their required bandwidth, that is, when users need low bandwidth, they can be associated. to RF. otherwise, they can associate to THz band. In addition, the handoff and mobility management algorithms will very crucial [55, 56] in mixed frequency networks.

4.2.3 Interference mitigation in THz Layer

Although THz band is distinguished with low interference due its directivity, it may imposes interference at the desired user of a BS. Thus, another direction to this work is the interference mitigation. Power allocation, which is an approach for interference mitigation RF and mmWave, can be applied in the system model provided in the thesis. Power allocation not only will decrease the interference, but also it will result in the efficient use of power resources.

4.2.4 THz for IoT Communications

High data rate and short-range communication is one of the paramount applications of THz BSs. As an example, consider the case when the number of users is extremely high in an area such as shopping malls, airport gates, and to name but three. Those users require high bandwidth, and by deploying THz base stations in these areas, the transmission of bulk data up to several Gbps is feasible for the moving users in a short time span in order of seconds. However, this use case has some challenges that needed to be addressed. Fast node association and authentication, well-timed content delivery to the serving base station, and caching the contents are among the challenges required to be taken into consideration in the design of future networks.

4.2.5 Secure THz communication

The intrinsic highly directional beam of THz band has the potential to provide secure communications, especially for military usage. For example, in the military usage, the directivity feature of the THz band can limit the accessibility to support different users such as soldiers, armoured personnel carriers, and tanks in a battlefield. Thus, in

comparison to the lower band frequencies, which are prone to the spoofing, THz band naturally suggests a secure communication only by the geometry of the network itself, which obviates the need for tasking encryption algorithms. Yet, in order to benefit from this feature of THz, beam alignment and beam tracking should be studied as well in the THz band.

Bibliography

[1] The evolution of mobile wireless communication technology: from 1G to 5G. [Online]. Available: https://twitter.com/5GBarcelona

[2] J. G. Andrews, A. K. Gupta, and H. S. Dhillon, "A primer on cellular network analysis using stochastic geometry," *arXiv preprint arXiv:1604.03183*, 2016.

[3] J. G. Andrews, S. Buzzi, W. Choi, S. V. Hanly, A. Lozano, A. C. Soong, and J. C. Zhang, "What will 5G be?" *IEEE Journal on Sel. areas in Commun.*, vol. 32, no. 6, pp. 1065–1082, 2014.

[4] H. Tabassum, A. H. Sakr, and E. Hossain, "Analysis of massive MIMO-enabled downlink wireless backhauling for full-duplex small cells," *IEEE Trans. on Commun.*, vol. 64, no. 6, pp. 2354–2369, 2016.

[5] Galaxy 10 specifications. [Online]. Available: https://www.samsung.com/global/galaxy/galaxy-s10/specs/

[6] M. Agiwal, A. Roy, and N. Saxena, "Next generation 5G wireless networks: A comprehensive survey," *IEEE Commun. Surveys Tutorials*, vol. 18, no. 3, pp. 1617–1655, 2016.

[7] A. Yastrebova, R. Kirichek, Y. Koucheryavy, A. Borodin, and A. Koucheryavy, "Future networks 2030: architecture & requirements," in *2018 10th International Congress on Ultra Modern Telecommunications and Control Systems and Workshops (ICUMT)*, 2018, pp. 1–8.

[8] H. Ibrahim, H. Tabassum, and U. T. Nguyen, "The meta distributions of the SIR/SNR and data rate in coexisting sub-6GHz and millimeter-wave cellular networks," *arXiv preprint arXiv:1905.12002*, 2019.

[9] H. Tabassum and E. Hossain, "Coverage and rate analysis for co-existing rf/vlc downlink cellular networks," *IEEE Trans. on Wireless Commun.*, vol. 17, no. 4, pp. 2588–2601, 2017.

[10] H. Elgala, M.-S. Alouini, H. Haas, M. Rahaim, H. Tabassum, and T. Watanabe, "Introduction to the special section on coexisting radio and optical wireless deployments (CROWD)," *IEEE Trans. on Cognitive Commun. and Networking*, vol. 5, no. 4, pp. 1178–1181, 2019.

[11] A.-A. A. Boulogeorgos, E. N. Papasotiriou, and A. Alexiou, "Analytical performance assessment of THz wireless systems," *IEEE Access*, vol. 7, pp. 11 436–11 453, 2019.

[12] H. Zhang, S. Huang, C. Jiang, K. Long, V. C. Leung, and H. V. Poor, "Energy efficient user association and power allocation in millimeter-wave-based ultra dense networks with energy harvesting base stations," *IEEE Journal on Sel. Areas in Commun.*, vol. 35, no. 9, pp. 1936–1947, 2017.

[13] C. Han and Y. Chen, "Propagation modeling for wireless communications in the terahertz band," *IEEE Commun. Magazine*, vol. 56, no. 6, pp. 96–101, 2018.

[14] K. Guan, B. Peng, D. He, J. M. Eckhardt, S. Rey, B. Ai, Z. Zhong, and T. Kürner, "Measurement, simulation, and characterization of train-to-infrastructure inside-station channel at the terahertz band," *IEEE Trans. on Terahertz Science and Technology*, vol. 9, no. 3, pp. 291–306, 2019.

[15] T. Bai, R. Vaze, and R. W. Heath, "Analysis of blockage effects on urban cellular networks," *IEEE Trans. on Wireless Commun.*, vol. 13, no. 9, pp. 5070–5083, 2014.

[16] I. K. Jain, R. Kumar, and S. S. Panwar, "The impact of mobile blockers on millimeter wave cellular systems," *IEEE Journal on Sel. Areas in Commun.*, vol. 37, no. 4, pp. 854–868, 2019.

[17] M. Gerasimenko, D. Moltchanov, M. Gapeyenko, S. Andreev, and Y. Koucheryavy, "Capacity of multiconnectivity mmwave systems with dynamic blockage and directional antennas," *IEEE Trans. on Vehicular Technology*, vol. 68, no. 4, pp. 3534–3549, 2019.

[18] V. Petrov, D. Solomitckii, A. Samuylov, M. A. Lema, M. Gapeyenko, D. Moltchanov, S. Andreev, V. Naumov, K. Samouylov, M. Dohler *et al.*, "Dynamic multi-connectivity performance in ultra-dense urban mmwave deployments," *IEEE Journal on Sel. Areas in Commun.*, vol. 35, no. 9, pp. 2038–2055, 2017.

[19] A. Shafie, N. Yang, and C. Han, "Multi-connectivity for indoor terahertz communication with self and dynamic blockage," *arXiv preprint arXiv:2004.07469*, 2020.

[20] P. Nain, D. Towsley, B. Liu, and Z. Liu, "Properties of random direction models," in *Proceedings IEEE 24th Annual Joint Conference of the IEEE Computer and Commun. Societies.*, vol. 3. IEEE, 2005, pp. 1897–1907.

[21] M. K. Mueller, M. Taranetz, and M. Rupp, "Analyzing wireless indoor communications by blockage models," *IEEE Access*, vol. 5, pp. 2172–2186, 2016.

[22] H. Zheng, J. Zhang, H. Hu, and J. Zhang, "The analysis of indoor wireless communications by a blockage model in ultra-dense networks," in *2018 IEEE 88th Vehicular Technology Conference (VTC-Fall)*. IEEE, 2018, pp. 1–6.

[23] J. M. Jornet and I. F. Akyildiz, "Channel modeling and capacity analysis for electromagnetic wireless nanonetworks in the terahertz band," *IEEE Trans. on Wireless Commun.*, vol. 10, no. 10, pp. 3211–3221, 2011.

[24] S. Mumtaz, J. M. Jornet, J. Aulin, W. H. Gerstacker, X. Dong, and B. Ai, "Terahertz communication for vehicular networks," *IEEE Trans. on Vehicular Technology*, vol. 66, no. 7, pp. 5617–5625, 2017.

[25] T. Kleine-Ostmann and T. Nagatsuma, "A review on terahertz communications research," *Journal of Infrared, Millimeter, and THz Waves*, vol. 32, no. 2, pp. 143–171, 2011.

[26] H.-J. Song and T. Nagatsuma, "Present and future of terahertz communications," *IEEE Trans. on terahertz science and technology*, vol. 1, no. 1, pp. 256–263, 2011.

[27] J. Kokkoniemi, J. Lehtomäki, and M. Juntti, "Stochastic geometry analysis for mean interference power and outage probability in THz networks," *IEEE Trans. on Wireless Commun.*, vol. 16, no. 5, pp. 3017–3028, 2017.

[28] J. Silvester and L. Kleinrock, "On the capacity of multihop slotted aloha networks with regular structure," *IEEE Trans. on Commun.*, vol. 31, no. 8, pp. 974–982, 1983.

[29] R. Mathar and J. Mattfeldt, "On the distribution of cumulated interference power in rayleigh fading channels," *Wireless Networks*, vol. 1, no. 1, pp. 31–36, 1995.

[30] V. P. Mhatre and C. P. Rosenberg, "Impact of network load on forward link intercell interference in cellular data networks," *IEEE Trans. on wireless Commun.*, vol. 5, no. 12, pp. 3651–3661, 2006.

[31] F. G. Nocetti, I. Stojmenovic, and J. Zhang, "Addressing and routing in hexagonal networks with applications for tracking mobile users and connection rerouting in cellular networks," *IEEE Trans. on Parallel and Distributed Systems*, vol. 13, no. 9, pp. 963–971, 2002.

[32] F. Baccelli and B. Błaszczyszyn, *Stochastic geometry and wireless networks.* Now Publishers Inc, 2010, vol. 1.

[33] B. Błaszczyszyn, M. Haenggi, P. Keeler, and S. Mukherjee, *Stochastic geometry analysis of cellular networks*. Cambridge University Press, 2018.

[34] M. Haenggi, *Stochastic geometry for wireless networks*. Cambridge University Press, 2012.

[35] V. Schmidt, *Stochastic geometry, spatial statistics and random fields*. Springer, 2014.

[36] S. Srinivasa and M. Haenggi, "Distance distributions in finite uniformly random networks: Theory and applications," *IEEE Trans. on Vehicular Technology*, vol. 59, no. 2, pp. 940–949, 2010.

[37] R. K. Ganti and M. Haenggi, "Interference and outage in clustered wireless ad hoc networks," *IEEE Trans. on Information Theory*, vol. 55, no. 9, pp. 4067–4086, 2009.

[38] C. Chaccour, R. Amer, B. Zhou, and W. Saad, "On the reliability of wireless virtual reality at terahertz (THz) frequencies," in *10th IFIP Int. Conf. on New Technologies, Mobility and Security (NTMS)*, 2019.

[39] X.-W. Yao, C.-C. Wang, and C.-F. Qi, "Interference and coverage analysis for indoor THz communications with beamforming antennas," in *IEEE/CIC Int. conf. on Commun. wkshps. in China*, 2019.

[40] K. Ntontin and C. Verikoukis, "Toward the performance enhancement of microwave cellular networks through THz links," *IEEE Trans. on Vehicular Technology*, vol. 66, no. 7, pp. 5635–5646, 2016.

[41] A. Moldovan, P. Karunakaran, I. F. Akyildiz, and W. H. Gerstacker, "Coverage and achievable rate analysis for indoor terahertz wireless networks," in *2017 IEEE International Conference on Commun. (ICC)*. IEEE, 2017, pp. 1–7.

[42] D. Liu, L. Wang, Y. Chen, M. Elkashlan, K.-K. Wong, R. Schober, and L. Hanzo, "User association in 5G networks: A survey and an outlook," *IEEE Commun. Surveys & Tut.*, vol. 18, no. 2, pp. 1018–1044, 2016.

[43] H. S. Dhillon, R. K. Ganti, and J. G. Andrews, "A tractable framework for coverage and outage in heterogeneous cellular networks," in *2011 Information Theory and Applications Workshop*. IEEE, 2011, pp. 1–6.

[44] H. S. Dhillon, R. K. Ganti, F. Baccelli, and J. G. Andrews, "Modeling and analysis of k-tier downlink heterogeneous cellular networks," *IEEE Journal on Sel. Areas in Commun.*, vol. 30, no. 3, pp. 550–560, 2012.

[45] H.-S. Jo, Y. J. Sang, P. Xia, and J. G. Andrews, "Heterogeneous cellular networks with flexible cell association: A comprehensive downlink SINR analysis," *IEEE Trans. on Wireless Commun.*, vol. 11, no. 10, pp. 3484–3495, 2012.

[46] Q. Ye, B. Rong, Y. Chen, M. Al-Shalash, C. Caramanis, and J. G. Andrews, "User association for load balancing in heterogeneous cellular networks," *IEEE Trans. on Wireless Commun.*, vol. 12, no. 6, pp. 2706–2716, Jun. 2013.

[47] J. Rubio, A. Pascual-Iserte, J. del Olmo, and J. Vidal, "User association strategies in HetNets leading to rate balancing under energy constraints," *EURASIP Journal on Wireless Commun. and Networking*, vol. 2017, no. 1, p. 204, 2017.

[48] Q. Ye, O. Y. Bursalioglu, H. C. Papadopoulos, C. Caramanis, and J. G. Andrews, "User association and interference management in massive MIMO HetNets," *IEEE Trans. on Commun.*, vol. 64, no. 5, pp. 2049–2065, 2016.

[49] A. Zappone, L. Sanguinetti, and M. Debbah, "User association and load balancing for massive MIMO through deep learning," in *2018 52nd Asilomar Conference on Signals, Systems, and Computers*. IEEE, 2018, pp. 1262–1266.

[50] C. Chaccour, M. N. Soorki, W. Saad, M. Bennis, and P. Popovski, "Can terahertz provide high-rate reliable low latency communications for wireless VR?" *arXiv preprint arXiv:2005.00536*, 2020.

[51] M. Di Renzo, "Stochastic geometry modeling and analysis of multi-tier millimeter wave cellular networks," *IEEE Trans. on Wireless Commun.*, vol. 14, no. 9, pp. 5038–5057, 2015.

[52] J. Gil-Pelaez, "Note on the inversion theorem," *Biometrika*, vol. 38, no. 3-4, pp. 481–482, 1951.

[53] I. S. Gradshteyn and I. M. Ryzhik, *Table of integrals, series, and products*. Academic press, 2014.

[54] L. S. Rothman, I. E. Gordon, A. Barbe, D. C. Benner, P. F. Bernath, M. Birk, V. Boudon, L. R. Brown, A. Campargue, J.-P. Champion *et al.*, "The HITRAN 2008 molecular spectroscopic database," *Journal of Quantitative Spectroscopy and Radiative Trans.fer*, vol. 110, no. 9-10, pp. 533–572, 2009.

[55] H. Tabassum, M. Salehi, and E. Hossain, "Fundamentals of mobility-aware performance characterization of cellular networks: A tutorial," *IEEE Commun. Surveys & Tutorials*, vol. 21, no. 3, pp. 2288–2308, 2019.

[56] H. Tabassum, E. Hossain, M. J. Hossain, and D. I. Kim, "On the spectral efficiency of multiuser scheduling in rf-powered uplink cellular networks," *IEEE Trans. on wireless Commun.*, vol. 14, no. 7, pp. 3586–3600, 2015.

Appendix A

Proofs of Chapter 3

A.1 Proof of Lemma 1

Recall that $I^{T}_{\text{agg}} = \sum_{\text{i}\in\Phi_T\setminus 0} P_{\text{T}} D_i h\left(r_i\right)$, after averaging over D_i the LT of the aggregate interference can be given as:

$$
\begin{aligned}
&\mathcal{L}_{I^{\text{T}}_{\text{agg}}}(s) = \mathbb{E}_{\Phi_T}\left[e^{-sI_{\text{agg}}}\right] = \mathbb{E}_{\Phi_T}\left[e^{-sF\sum_{i\in\Phi_T\setminus 0} P_{\text{T}}\gamma_T \frac{e^{-k_a(f)r_i}}{r_i^2}}\right],\\
&= \mathbb{E}_{\Phi_T}\left[\prod_{i\in\Phi_T\setminus 0} \exp\left(-sFP_{\text{T}}\gamma_T \frac{e^{-k_a(f)r_i}}{r_i^2}\right)\right],\\
&\overset{(a)}{=} \exp\left(-2\pi\lambda_T \int_r^{\infty} r_i \left(1-\exp\left(-s\gamma_T F P_{\text{T}} \frac{e^{-k_a(f)r_i}}{r_i^2}\right)\right) dr_i\right),\\
&\overset{(b)}{=} \exp\left(-2\pi\lambda_T \int_r^{\infty} \sum_{l=1}^{\infty} \frac{\left(-s\gamma_T F P_{\text{T}}\right)^l \exp\left(-lk_a\left(f\right) r_i\right)}{r_i^{2l-1} l!} dr_i\right),\\
&\overset{(c)}{=} \exp\left(-2\pi\lambda_T \sum_{i=1}^{\infty} \frac{\left(-s\gamma_T P_{\text{T}}\right)^i}{i!} \left[-\left(ik_a\left(f\right)\right)^{2(i-1)} \Gamma\left(-2(i-1), ik_a\left(f\right) r\right)\right]_r^{\infty}\right)\\
&\overset{(c)}{=} \exp\left(2\pi\lambda_T \sum_{l=1}^{\infty} \frac{\left(-s\gamma_T F P_{\text{T}}\right)^l}{\left(lk_\alpha\left(f\right)\right)^{2-2l} l!} \Gamma\left(2-2l, lk_a\left(f\right) r\right)\right),
\end{aligned}
$$

where (a) is derived by using the probability generating functional (**PGFL**) with respect to $f(x) = \exp\left(-sP_T h\left(r_i\right)\right)$, (b) is derived using $\exp\left(-x\right) = \sum_{i=0}^{\infty}(-1)^i \frac{x^i}{i!}$ ([53],

Eq. 1.211), and (c) follows from the integral identity $\int \frac{\exp(-\beta x^n)}{x^m} dx = -\frac{\beta^z \Gamma(-z, \beta x^n)}{n}$, and z equals to $\frac{m-1}{n}$ ([53], Eq. 2.345). Since the typical user has a distance r from its serving TBS due to the nearest BS association, all interferers exist beyond r. Thus, the lower limit in the integral is r.

A.2 Proof of Lemma 2

The distribution of the distances between the typical user and its nearest THz and RF BSs are $f_r(r) = 2\pi\lambda_T r \exp\left(-\pi\lambda_T r^2\right)$ and $f_\rho(\rho) = 2\pi\lambda_R \rho \exp\left(-\pi\lambda_R \rho^2\right)$, respectively. Thus, averaging over r in (3.6) yields the association probability[1] with TBS as:

$$
\begin{aligned}
\mathcal{P}_{A_T} &= \int_0^\infty \exp\left(-\pi\lambda_R \left(Kr^2\right)^{\frac{2}{\alpha}} \exp\left(\frac{2k_a\left(f\right) r}{\alpha}\right)\right) f_r(r) dr, \\
&\overset{(a)}{=} \int_0^\infty 2\pi\lambda_T \alpha h^{2\alpha-1} e^{-\pi\lambda_T h^{2\alpha}} \exp\left(-\pi\lambda_R K^{\frac{2}{\alpha}} h^4 e^{\frac{2k_a(f)h^\alpha}{\alpha}}\right) dh, \\
&\overset{(b)}{=} \int_0^\infty 2\pi\lambda_T \alpha h^{2\alpha-1} e^{-\pi\lambda_T h^{2\alpha}} \sum_{j=0}^{\infty} \frac{\left(-\pi\lambda_R K^{\frac{2}{\alpha}} h^4 e^{\frac{2k_a(f)}{\alpha}h^\alpha}\right)^j}{j!} dh, \\
&= \sum_{j=1}^{\infty} \frac{(-1)^j}{j!} \int_0^\infty 2\pi\lambda_T \alpha \left(\pi\lambda_R \left(\frac{\gamma_R}{\gamma_T}\right)^{\frac{2}{\alpha}}\right)^j h^{2\alpha-1} h^4 \\
&\overset{(c)}{=} \sum_{j=0}^{\infty} \frac{\left(-\pi\lambda_R K^{\frac{2}{\alpha}}\right)^j}{j!} \int_0^\infty 2\pi\lambda_T z^{\frac{4j+\alpha}{\alpha}} e^{-\pi\lambda_T z^2 + \frac{2jk_a(f)}{\alpha} z} dz, \\
&= \sum_{j=0}^{\infty} \frac{\left(-\pi\lambda_R K^{\frac{2}{\alpha}}\right)^j}{j!} \int_0^\infty 2\pi\lambda_T z^{v_j - 1} e^{-\beta z^2 - \eta_j z} dz, \\
&\overset{(d)}{=} \sum_{j=1}^{\infty} \frac{(-1)^j}{j!} \delta_j \left(2\beta\right)^{-\frac{v_j}{2}} \Gamma\left[v_j\right] \exp\left(\frac{-\eta_j}{8\beta}\right) D_{-v_j}\left(\frac{-\eta_j}{\sqrt{2\beta}}\right)
\end{aligned}
$$

where (a) is derived by changing variables $r = h^\alpha$, (b) follows from expanding the exponential function as $\exp\left(-x\right) = \sum_{i=0}^{\infty} (-1)^i \frac{x^i}{i!}$ ([53], Eq. 1.211), (c) follows from

[1] User association to a BS is a slowly varying process that relies on long-term channel propagation factors such as path-loss and shadowing.

the variable change $z = h^{\alpha}$, and, finally, **Lemma 2** is derived by using the integral identity $\int_0^{\infty} x^{\nu-1} e^{-\beta x^2 - \eta x} dx = (2\beta)^{-\frac{\nu}{2}} \Gamma[\nu] \exp\left(\frac{\eta^2}{8\beta}\right) D_{-\nu}\left(\frac{\eta}{\sqrt{2\beta}}\right)$ ([53], Eq. 3.462).

A.3 Proof of Lemma 3

The distribution of the distance from the tagged BS in the tier k where $k = \{\text{THz}, \text{RF}\}$ can be derived as follows:

$$\begin{aligned} f_{\hat{X}_k}(\hat{x}) =& \frac{d\Pr[\hat{X}_k > \hat{x}]}{d\hat{x}} = \frac{d\Pr[X_k > \hat{x} | k = n]}{d\hat{x}} \\ =& \frac{d\Pr[X_k > \hat{x}, k = n]}{\Pr[k = n] d\hat{x}}, \end{aligned} \tag{A.1}$$

where $n \in \{\text{THz}, \text{RF}\}$ is the index of the layer to which a user will associate. $\Pr[k = n]$ is the association probability of a user to tier k as given in **Lemma 2**. When the user associates to the TBS, the numerator in (A.1) can be given as:

$$\begin{aligned} &\Pr[X_T > \hat{x} | k = \text{THz}] = \Pr[X_T > \hat{x}, B_T P_r^{\text{THz}} > P_r^{\text{RF}}], \\ &= \int_{\hat{x}}^{\infty} \Pr[B_T P_r^{\text{THz}} > P_r^{\text{RF}}] f_{X_T}(x) dx, \\ &\overset{(a)}{=} \int_{\hat{x}}^{\infty} 2\pi\lambda_T x e^{-\pi\lambda_R K^{2/\alpha} x^{4/\alpha} e^{2k_a(f)x/\alpha} - \pi\lambda_T x^2} dx, \end{aligned} \tag{A.2}$$

where (a) is derived by substituting $\Pr[P_r^{\text{THz}} > P_r^{\text{RF}}]$ provided in **Appendix B**, and $f_{X_T}(x) = 2\pi\lambda_T x \exp(-\pi\lambda_T x^2)$. Now substituting (A.2) in (A.1) results in $f_{\hat{X}_T}(\hat{x})$.

Likewise, when the user associates to the RF layer, then:

$$
\begin{aligned}
&\Pr[X_R > \hat{x} | k = \mathrm{RF}] = \Pr[X_R > \hat{x}, P_r^{\mathrm{RF}} > B_T P_r^{\mathrm{THz}}], \\
&= \int_{\hat{x}}^{\infty} \Pr[P_r^{\mathrm{RF}} > B_T P_r^{\mathrm{THz}}] f_{X_R}(x) dx, \\
&= \int_{\hat{x}}^{\infty} \\
&= \int_{\hat{x}}^{\infty} \Pr\left[\pi r^2 \exp\left(k_a\left(f\right) r\right) > K x^{\alpha}\right] f_{X_R}(x) dx, \\
&\overset{(a)}{\approx} \int_{\hat{x}}^{\infty} \Pr\left[r > \left(\frac{K x^{\alpha}}{\pi}\right)^{\frac{1}{2+\mu}}\right] f_{X_R}(x) dx, \\
&= \int_{\hat{x}}^{\infty} 2\pi\lambda_R x \exp\left(-\pi\lambda_T \left(\frac{K x^{\alpha}}{\pi}\right)^{\frac{1}{2+\mu}} - \pi\lambda_R x^2\right) dx,
\end{aligned}
\tag{A.3}
$$

where (a) is derived by approximating $r^2 \exp\left(k_a\left(f\right) r\right)$ with $r^{2+\mu}$, and μ is a correcting factor. That is, when $k_a\left(f\right) > 0.1$ than $\mu = 2 + \frac{10 k_a(f)}{1+2k_a(f)}$, otherwise $\mu = 2 + \frac{15 k_a(f)}{1+10k_a(f)}$. Finally, substituting (A.3) in (A.1) results $f_{\hat{X}_R}(\hat{x})$.